A Tall Ship and a Star to Steer Her By

A Phase I NIAC Award to solicitation NNH15ZOA001N-15NIAC-A1
Project number: NNX15AL83G
Final Report
February 7, 2016

Principal Investigator: Michael Hecht (MIT Haystack Observatory)
Co-Investigators:
Kerri Cahoy (MIT Aero-Astro)
Vincent Fish (MIT Haystack Observatory)
Student Investigator: Hyosang Yoon (MIT Aero-Astro)
Collaborators: Tomas Svitek (Stellar Explorations, Inc.)
Key Staff: Frank Lind (MIT)

A Tall Ship and a Star to Steer Her By
Michael Hecht / MIT Haystack Observatory

Concept

- Differential Deployable Autonomous Radio Navigation (ΔDARN)
- A deployable phased array antenna provides celestial velocity (from astronomical masers) and position (from pulsars)
- No mechanical pointing; Double use for telecom

Study Approach

- Develop catalog of maser sources suitable for navigation
- Conceptual design of ultra-light deployable phased-array telescope
- System analysis, roadmap, and outline of demonstration mission

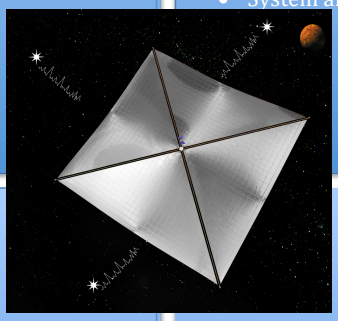

Benefits

- Autonomous or near-autonomous navigation without mechanical pointing
- Powerful phased array antennas for communication and science
- Possible common device for navigation, communication, and propulsion

Evaluation Notes

Table of Contents:

1 EXECUTIVE SUMMARY 4

1.1 BROAD OBJECTIVES: 4
1.2 PROPOSED APPROACH: 4
1.3 FINDINGS 5
1.3.1 RNAV WITH MASERS 5
1.3.2 RNAV WITH PULSARS 6
1.4 NEXT STEPS 6

2 OVERVIEW AND HISTORY 7

2.1 GEODETIC PERSPECTIVE 7
2.2 SPACECRAFT NAVIGATION 7
2.3 WHY AUTONOMY? 8
2.4 QUASARS, MASERS, AND PULSARS 8
2.5 NATURE OF THE STUDY 10
2.6 SCOPE OF THE INVESTIGATION 11

3 SIMULATION (MASERS) 12

3.1 SPECTRAL ANALYSIS 12
3.1.1 CROSS CORRELATION 13
3.2 SIMULATION RESULTS 15
3.2.1 APPROACH 15
3.2.2 LIMITATIONS OF THE APPROACH 17
3.2.3 SIMULATION WITH COVARIANCE ANALYSIS: 17
3.2.4 SIMULATION CONCLUSIONS 19

4 OBSERVATIONS AND ANALYSIS (MASERS) 20

4.1 REVIEW OF LITERATURE 20
4.2 TARGET SOURCES 20
4.3 RESULTS 23
4.4 CONCLUSIONS FROM OBSERVATIONS 24

5 SPACE-BASED RNAV VALIDATION (MASERS) 25

5.1 ORBIT CONSIDERATIONS 25
5.2 CONCEPT OF OPERATIONS 26
5.3 BASELINE DESIGN 27
5.4 SUBSYSTEM DESIGN 29
5.4.1 COMMUNICATIONS 29
5.4.2 ELECTRICAL POWER SYSTEM 29
5.4.3 COMMAND AND DATA HANDLING 30
5.4.4 GUIDANCE, NAVIGATION, AND CONTROL 31
5.4.5 STRUCTURE 33
5.4.6 PROPULSION 34
5.5 ANTENNAS 35
5.5.1 TRADES 35

5.5.2 TALLCUBE DESIGN CHOICE 36
5.6 SIGNAL PROCESSING 37

6 THE CASE FOR PULSARS 38

6.1 APPROACH 38
6.2 IN-SPACE VALIDATION 40

7 REFERENCES 43

1 Executive Summary

The vision: Sailing ships once navigated by the fixed stars and a nautical chronometer. Untethered from the terrestrial reference frame, future spacecraft will require more than a star chart to accomplish the same feat; instead, they may exploit the peculiar time and frequency structure of light from those distant stars to autonomously or semi-autonomously determine their position and velocity in the celestial reference frame

1.1 Broad Objectives:

Two visionary innovations were proposed to allow spacecraft to assume the burden of navigation. The first extends the International Celestial Reference Frame (ICRF) to include not only *orientation* references (quasars), but also time (pulsars) and frequency (maser) references that allow *position* and *velocity* to be determined relative to the terrestrial reference frame (TRF) or planetary reference frames (PRFs). The second provides spacecraft with a direct means to determine their *own* position relative to the ICRF.

1.2 Proposed approach:

The inspiration for the Tall Ship proposal was the progress being made towards using time-of-arrival (TOA) and Doppler shift *x-ray* signatures of millisecond pulsars in support of autonomous spacecraft navigation. This technique, sometimes dubbed XNAV, will be tested at a proof-of-concept level as part of the upcoming NICER/SEXTANT experiment on the International Space Station (Arzoumanian et al. 2014).

While XNAV is promising, the x-ray signal from pulsars is intrinsically weak, the detection instrumentation is cumbersome and single-purpose, and the overall resource burden on small spacecraft is likely to be large even after projecting the technology forward in time. In that respect, analogous techniques implemented using radio methods in the microwave bands (what might be called RNAV) may be preferable. The signal-to-noise ratio of the sources is higher in the microwave, the technology better lends itself to miniaturization, and large radio antennas and receivers are more synergistic with other spacecraft subsystems in the sense that they can contribute towards communication, and can share collecting area with a solar power system. Electronic beamforming technology will potentially reduce most of the pointing burden on the spacecraft as it matures, and (as described here), bright and ubiquitous astronomical masers, which provide frequency references for Doppler measurements, may complement or even replace the rare and difficult-to-detect pulsars as catalogue sources.

The Tall Ship team therefore proposed to observationally determine, first, whether well-known astronomical masers are sufficiently stable on short time scales to constitute an ICRF sub-catalog that can be used for spacecraft navigation. Second, we proposed to assess the scope of spacecraft resources that would be required to exploit such a catalog, including antenna area, deployment mechanisms, power, and computational capability. Finally, we proposed to explore deployment of even larger antennas from small spacecraft that would be able to utilize both pulsars and masers for navigation.

1.3 Findings

By way of overall summary, the prospect of autonomous navigation with astronomical masers proved less inviting in light of the Phase I research findings, but the prospect of using radio *pulsars* was significantly improved. The difference in the degree of difficulty is nowhere near as great as initially expected, and the navigational value of radio pulsar signals is found to be significantly greater. Moreover, a straightforward and inexpensive path to flight validation was identified.

1.3.1 RNAV with masers

Despite the need for an extra integral to extract position information from Doppler shifts, we originally focused on astronomical masers because of the relative simplicity of detection, the ubiquity of bright sources, and the opportunity to use relatively small antennas to detect bright sources in the 3-30 mm (10-100 GHz) range. Initial estimates of signal strength suggested that 1 m^2 would be adequate antenna area, a size nominally compatible with a CubeSat.

Observations: Initial observations using the Haystack Observatory 37 meter telescope suggested that from an overall system-to-noise (SNR) perspective, water masers at 22 GHz were a better target than SiO masers at 43 GHz for a similar size antenna. Subsequent observations focused on studying the stability or predictability of spectral features at various times scales. In general, it was founded that on relatively short time scales (hours to days), frequency shifts of peaks did not exceed 20-30 m/s. While encouraging, this finding still lacks an order of magnitude or more of the precision needed to achieve the desired system performance for RNAV. However, strong evidence suggested that most of the residual changes were the result of instrumental error, and work continues both on improving the instrumentation and identifying features and patterns in the spectra that will further reduce the uncertainty.

Antenna design: Purely from the perspective of performance, phased array antennas are appealing for RNAV because steering can be done totally electronically. Initial assessments, however, suggested that the corresponding power penalty of simultaneously processing signals from many antenna elements was unfavorable, and ***reflectarray*** technology is a more practical approach from a system perspective. Reflectarrays use many passive elements focused on a single feed to achieve the advantage of deployment on a flat surface without the power penalty. Reflectarrays offer a large upside potential as *electromechanical* methods of beamforming mature, and eventually they may offer steerability comparable to a phased array without the power penalty. In the short term, they offer performance comparable to a parabolic dish, but can be integrated into flat solar arrays (either on the back or, in a transparent configuration, on the front) with a negligible mass and volume penalty on the spacecraft.

Scaling of the actual Haystack maser observations to a small space-based antenna suggests that the originally postulated 1-m^2 antenna was overly optimistic, and that an aperture of at least 4 m^2 is required to achieve the SNR needed to maintain positional accuracy of 10-20 km after a few months, even with ideal stable sources. While a factor of 2 in linear dimension seems modest, anything larger than a meter on a side is challenging for CubeSat implementation.

Compounding the difficulty is the surface figure that must be maintained for quality measurements, typically considered to be $1/15^{th}$ of a wavelength, or ~1mm at 22 GHz. This degree of surface control implies a level of stiffness, and hence mass, that isn't found in typical CubeSat solar panels. In theory, flaws in the figure can be calibrated *in situ* and compensated by tuning the antenna elements, but this capability has not yet been realized in lightweight space-based arrays.

1.3.2 RNAV with pulsars

While astronomical masers only allow determination of the instantaneous velocity vector of a spacecraft, detection of time-of-arrival and Doppler shift of radio pulsars, particularly msec-scale pulsars, provides a direct determination of instantaneous position.

At the time of submission of the Phase I proposal, the literature suggested that a capable pulsar-detection system required of order 100 m^2 antenna aperture, and imposed mass and power requirements that exceeded the capability of small satellites Becker et al (2013). More recent studies out of the same group (Jessner 2016), now suggest that the power and computational issues are modest, and an antenna size of 30-40 m^2 (i.e. about 3x the diameter of the maser antenna) will be sufficient for detection. Moreover, at the recommended frequency of ~500 MHz, the antenna may consist of a lightweight mesh, and surface errors of 5-10 cm can be tolerated.

As a result, we can consider relatively flimsy structures for pulsar detection that weigh no more than antennas for maser detection, and are substantially more tolerant to distortion. From a system perspective, this may prove simpler and less resource intensive to implement, with vastly superior navigational results.

1.4 Next steps

The overall conclusion of this work is that radio navigation (RNAV) using *pulsar* signals in the UHF band is extremely promising in the near-term; the original maser focus of this work offers a potentially useful augmentation, though it faces near-term challenges in accommodating the precision antenna.

The RNAV concept is most readily validated in the near term by leveraging existing assets, using data from Radio Astron, a 10-meter space-based telescope currently in a high orbit around Earth (Kardashev et al. 2012). Designed primarily for Very Long Baseline Interferometry (VLBI), Radio Astron is equipped with high precision timing and its absolute position is known to great accuracy. Should a Phase II effort be awarded, we proposed to independently demonstrate determination of Radio Astron position using existing or new pulsar timing data.

Using new and existing technology, we also describe in this report a dedicated RNAV demonstration featuring a large-area deployable antenna developed by our partner Stellar Exploration, Inc. on a small satellite that would be deployed on a cis-lunar or deep space trajectory.

2 Overview and history

Deep space travel would be significantly more affordable and widely accessible if spacecraft could guide themselves to their destinations. Steering by the stars and a precise clock, as we've long done on Earth, is not possible without the fixed reference frame of the Earth's surface. But certain stars, the fast (msec) *pulsars*, are natural GPS beacons, and by timing the arrival and separation of their pulses it is possible for a spacecraft to autonomously determine its position and velocity. Other stars, the more common and brighter astronomical *masers*, emit fixed frequency tones that can be used to determine velocity only. Currently one experiment, NICER/SEXTANT, is exploring the use of x-ray pulsar data for navigation by flying a large x-ray detector on the ISS, a technique called XNAV. In the Phase I of Tall Ship, we explored using radio waves instead, a technology we believe is more accurate and better suited to the CubeSat-scale spacecraft of the future. While Phase I emphasized maser observations, the results pointed strongly towards a future emphasis on *pulsars*.

2.1 Geodetic perspective

Since the beginning of recorded history, navigation has been accomplished with the aid of a terrestrial reference frame (TRF) in the form of maps and landmarks; a celestial reference frame (CRF) in the form of star charts; and to tie them together, Earth orientation parameters (EOP) in the form of time-keeping devices or the known motions of the sun, moon, and planets.

Contemporary needs for precise navigation, whether for guiding spacecraft to the stars or projectiles to their terrestrial destinations, and for precision metrology to measure quantities such as sea level rise or tectonic activity, have driven geodetic science to new heights of accuracy. While we are accustomed to thinking of GPS (or, more properly, GNSS) as the ultimate navigational guide, underlying it is an international infrastructure, exemplified by NASA's Space Geodesy Project (SGP), that constantly refines and updates the TRF, CRF, and EOP so that the GPS satellites themselves know where they are (Plag and Pearlman, 2010). On the required TRF scale of millimeters or less, the Earth is a dynamic object, locally rising and falling in response to tides, glacial rebound, hydrology, and tectonics. The CRF itself must be constantly monitored and updated, as the spatial structure of electromagnetic radiation from distant quasars varies measurably. The EOP cannot be determined by timepieces alone, as the Earth wobbles on its axis and even slows or accelerates measurably due to the varying angular momentum of the atmosphere. Thus UT1 and other EOPs are regularly updated by astronomical measurements for use in Earth sciences and navigation of all types.

Deep space navigation ultimately calls for tying a spacecraft reference frame (SRF) to planetary reference frames (PRFs) that define the location of solar system objects. The PRFs have been tied to the TRF by a combination of optical observations, modeling, radar ranging measurements (and laser ranging in the case of our moon), and precision tracking of spacecraft in planetary orbits. Thus, with ties in place between the TRF, CRF, and PRFs, deep space navigation may be accomplished by linking the SRF to any of the three types of frames.

2.2 Spacecraft navigation

Advancement over state of art: The New Millennium Program's Deep Space 1 mission in the late 1990's represented the first attempt at autonomous navigation. Using purely optical and inertial methods, DS1 achieved a positional accuracy of ± 250 km and velocity accuracy of ±0.2 m/s. Speculatively, X-ray pulsar navigation promises 5-10 km accuracy (Becker et al. 2013). With RNAV, we aim to achieve <1 m/s velocity accuracy from masers and <5 km accuracy from pulsars. A notable advantage of radio detection over x-ray detection is the anticipated dual-use of radio antennas for navigation and communication. In future, since beamforming antennas (phased

arrays or reflectarrays with tunable elements) eliminate the need for pointing, a single deployed solar sail may be used for propulsion, navigation, communication, and power.

2.3 Why autonomy?

The goal of RNAV is to decimate, but not eliminate the bandwidth of Earth-to-spacecraft communication. We propose to accomplish this by replacing remote navigation services such as Doppler ranging by a *reference frame* service that can be provided to spacecraft in a compact form; much as national and international organizations transparently provide that service to spacecraft tracking stations like the DSN, or to GNSS satellites. *To exploit that minimal service, the spacecraft must have the ability to independently determine its position and orientation relative to the CRF (or, in close encounter, a PRF). That linkage is the subject of Tall Ship.*

With spacecraft components and "kits" becoming commodities available even to small university groups, advances in low thrust propulsion (e.g. Micci and Ketsdever 2000) and optical communication (e.g. Powell 2013) have brought closer the day when small, inexpensive probes will ply the interplanetary spaceways. Recent conferences and workshops have been dedicated to the prospect of deep space CubeSats alone (see, for example, www.iCubeSat.org).

At present, however, the infrastructure for deep space navigation is an expensive bottleneck to ubiquitous access to deep space. While star trackers provide attitude and crude position information, and inertial guidance units provide short-term velocity and position information, ultimately deep space navigation depends on two-way Doppler and ranging measurements from Earth. A giant leap in the accessibility of deep space exploration will occur when near-autonomous navigation becomes a reality. Not only does this break the tether to Earth, but it also enables exploration beyond the line of sight to Earth – behind planets, the sun, or even in interstellar space.

2.4 Quasars, masers, and pulsars

Quasars, whose locations comprise the ICRF, are strong, compact extragalactic objects that exemplify the notion of a "star chart" as a collection of point sources at infinite distance (Fig. 2-1). Intrinsically, such sources can only inform orientation.

While a good start chart is sufficient to monitor wander of the Earth's axis, it does not suffice, for example, to determine the scale of the Earth and other TRF parameters. Those needs are most readily met with a celestial timing reference against which to measure transmission delays. Very Long Baseline Interferometry (VLBI) is a sort of sleight-of-hand that allows a quasar to serve as a time-reference even though it has no explicit time structure. Developed by pioneers at MIT Haystack Observatory and elsewhere, VLBI exploits the fact that radio noise from quasars is coherent, and observations from different locations may be correlated to determine phase delays down to the picosecond level. With a sufficiently accurate common clock, typically a hydrogen maser, enormous datasets consisting entirely of time-stamped noise can be correlated and Fourier-transformed to form images of the quasars or, equivalently, to precisely locate the observatories (or spacecraft tracking stations) in the TRF.

VLBI has refined the accuracy of the ICRF and the corresponding EOPs to <1 nrad, corresponding to scale precision better than 1 ppb and location of TRF coordinates to <1 mm. A variant of VLBI, Delta Differential One-Way Ranging (ΔDOR) correlates transmissions from spacecraft and nearby quasars (in an angular sense), measured at widely spaced locations on Earth, to locate spacecraft to 1 nrad on the plane of the sky (PoS) (Curkendall & Border 2013). Combined with Doppler ranging, this technique can place a spacecraft within meters relative to solar system objects.

While the success of ΔDOR underscores the value of including time references in the ICRF, the exploitation of coherent quasar noise is of no direct value in autonomous spacecraft localization. Aside from the lack of a baseline against which to measure, the sheer volume of data that must be transmitted and correlated would make the technique more energy and bandwidth-intensive than the current Earth-based methods. Fortunately, nature offers an explicit time reference in ***pulsars***. These fairly rare objects (~2200 known) have periods ranging from milliseconds to seconds, and are thought to be spinning, strongly magnetized neutron stars with misaligned spin and magnetic axes. Pulsars are best observed in the UHF band, as intensity falls off rapidly with frequency, and antennas must be fairly large.

Figure 2-1: Artist's rendering of quasar ULAS J1120+0641. Credit: ESO/M. Kornmesser

Prior to this work, the best hope to achieve autonomous navigation was X-ray pulsar navigation (XNAV). This is a technique in which millisecond pulsar signals are compared to an absolute time reference to determine (relative) position by analysis of phase lags, and relative velocity by analysis of period changes resulting from the Doppler effect. While longer-period pulsars also provide timing information, it becomes increasingly difficult to determine time-of-arrival to high precision as the period increases. Progress in XNAV has been sufficiently encouraging that NASA has approved an ISS experiment, NICER/SEXTANT (N/S), to test the technology in space (Anderson and Pines 2013). Approximately fifty msec-scale pulsars are known to be observable in the soft x-ray. N/S will explore their value as navigational references with a compact, ~10 kg x-ray imaging system.

But while x-ray navigation is promising, the superiority of *radio* pulsar observations for navigation is widely acknowledged (Becker et al. 2013). Radio signatures are sharper in time (Fig. 2-2), have better signal-to-noise ratio, have far better angular resolution, and the number of pulsars to choose from is greater than in the x-ray. Moreover, if an antenna with beamforming capability, such as a phased array, is used for the radio dish, then the need for mechanical pointing of the telescope can be eliminated. The *impediment* to radio implementation has traditionally been the size of the dish required for the measurement (previously estimated at 10 m. diameter) and the mass, volume, and power demand of support components.

Pulsars are neither perfect clocks nor perfect point sources. Pulsar motion associated with galactic rotation, as well as their peculiar local motion relative to the galaxy, must be monitored, and pulsar navigation will require regular CRF updates. Pulsar frequencies also slowly evolve and occasionally jump, then slowly degrade to their nominal value.

Astronomical ***masers*** are common, strong sources of microwave emission that radiate in narrow frequency bands due to pumping and stimulated emission of molecular lines in stellar envelopes (Fig. 2-3). Like pulsars, masers are relatively nearby and their emission has measurable spatial structure, so they are not ideal fixed, point sources. Moreover, the maser spectral signature is known to vary significantly due to changing red and blue shifts, though the detailed time structure of this variation is *not* known (and is a subject of this study).

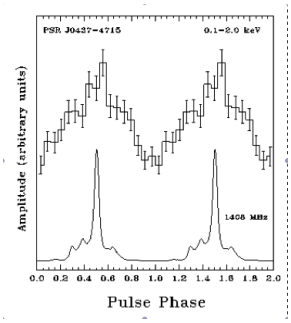

Figure 2-2: Radio vs. x-ray pulsar line comparison (from *Becker et al. 2013*)

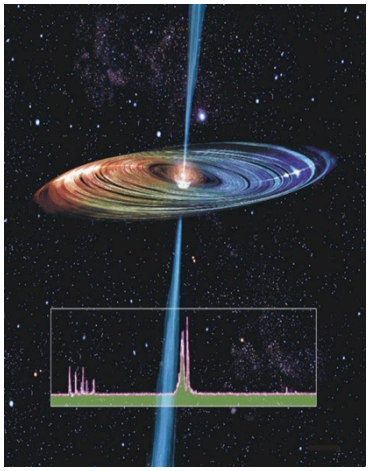

Figure 2-3: Water maser in NGC 4258. Image courtesy of NRAO/AUI and Artist: John Kagaya (Hoshi No Techou)

Unique to radio detection, the Doppler shift of maser spectra may be used to determine the spacecraft velocity vector relative to the PRFs with far smaller apertures than required for pulsar-based navigation (Dong et al. 2011). Not only does the maser measurement directly reveal the spacecraft heading, but only a single integration is required to determine position; a major improvement in accuracy over inertial accelerometers, which require a double integration. All that is required is a relatively small antenna and constantly updated knowledge of maser positions and spectral lineshapes.

For larger spacecraft, maser-based velocity determination can be complemented with large-aperture pulsar-based positioning, as well as inertial acceleration, and optical orientation tracking.

2.5 Nature of the study

Tall Ship explores the feasibility of an autonomous navigation technique based on radio detection of stellar objects that, by analogy to XNAV might be termed RNAV.

One goal was to observationally determine whether well-known astronomical masers are sufficiently stable on short time scales to constitute an ICRF sub-catalog that can be used for spacecraft navigation, and to assess the scope of spacecraft resources that would be required to exploit

such a catalog, including antenna area, deployment mechanisms, power, and computational capability. The second goal was to explore deployment of even larger antennas from small spacecraft that would be able to utilize pulsars for navigation.

2.6 Scope of the Investigation

Both pulsars and astronomical masers are potential tools of autonomous navigation. This study focused initially on the masers, which are both more common and much brighter than pulsars. Masers are narrow *frequency* sources whose Doppler shifts sensitively indicate relative velocity of a spacecraft. Prior literature, however, called into question the repeatability of the measured maser spectral shape on a time scale of hours to weeks. The absence of this knowledge is due, in part, to the fact that nobody has previously framed an application that might exploit such a property. In part it is due to the scarcity of observing time on appropriate radio telescopes, making such a time-resolved analysis impractical. While not an insurmountable problem (updated spectral parameters can be uploaded occasionally from the ground to enable corrections), it is important to understand the communication overhead imposed by this factor.

To assess the feasibility of establishing a maser catalog for the ICRF, we therefore examined the time stability of the spectrum of a small number of candidate masers using the 37 m. radio telescope at Haystack Observatory. We then utilized this information to constrain the size, mass, and processing power required for an antenna capable of measuring the maser spectrum (or pulsar time structure) with the required signal to noise ratio.

3 Simulation (masers)

The rest frequency of each masing transition is accurately known, and therefore can provide a velocity reference frame. Observed maser lines are Doppler shifted from the rest frequency due to line-of-sight motions between the masing material and the observer. If the Doppler shift of a maser feature measured on the ground is relayed to a spacecraft, the same maser feature can be observed from the spacecraft, and its Doppler shift relative to the ground value provides a measure of its line-of-sight velocity with respect to the ground.

A back-of-the-envelope analysis (Fig. 3-1), indicates that a meter-scaled phased array antenna provides sufficient signal to noise ratio (SNR) to resolve Doppler shifts of a maser spectrum with cm/sec precision. This analysis begins with a spectral line of characteristic width, typically of order 1 km/s, with detection noise characteristic of a short observation on Earth compared to a longer observation on a spacecraft. The desired outcome is spacecraft correlation to the reference spectrum with a fidelity of order 0.1 m/s. From a noise standpoint alone, the simulation suggests that correlation to a few cm/s is feasible.

To better determine the accuracy of the autonomous velocity estimation from a spacecraft, we began with actual maser spectra acquired by different telescopes, including the Haystack Observatory 37m telescope, and adjusted the signal-to-noise ratio (see box) to simulate what the spectra would have looked like had they been acquired by a small antenna, either 1 m^2 or 4 m^2 in accuracy. The simulated data was then analyzed using approaches described in the next Section.

To simulate the spectrum from a small dish, we interpolated the measured high signal-to-noise-ratio (SNR) data from ground-based telescopes to a 1kHz sampling frequency, then added equivalent noise as determined by the formula in the following box. Implicitly, this assumes the high-SNR measured data contains no noise, so the result may slightly underestimate the performance of an actual small antenna.

The noise of a radio telescope is described by its system equivalent flux density (SEFD),

$$SEFD = \frac{2kT_{sys}}{A_{eff}} = \frac{2kT_{sys}}{\eta A_{ant}} \quad (1)$$

where k is Boltzmann's constant, T_{sys} is the system temperature, and A_{eff} is the effective area (the geometric antenna area A_{ant} times the antenna efficiency η, a factor that is typically ~ 0.5 for a parabolic reflector). The RMS thermal noise with an antenna is

$$\sigma = x\frac{SEFD}{\sqrt{2BWt}} \quad (2)$$

where x is a sampling efficiency factor, close to but less than 1, BW is a channel bandwidth, and t is the integration time. This thermal noise is assumed to be an additive white Gaussian noise on a maser spectrum.

3.1 Spectral analysis

If the maser spectrum and associated sky background sources are constant from measurement to measurement, then changes with spacecraft velocity due to a Doppler shift are reflected in a rigid shift; the spectra would be otherwise identical except for random noise terms. To the extent that this is true, then the Doppler shift is best extracted with a simple cross correlation (CC) between the two spectra. This assumption was made for purposes of simulation.

3.1.1 Cross Correlation

Finding the maximum peak position of the cross-correlation is the optimal method to determine a rigid shift in the sense of least square estimation, as shown in the box on the following page. The upper plot of Fig. 3-2 shows a sample maser spectrum template and simulated measurement with a Doppler shift of 10 km/sec. The Doppler shift of the measurement is then estimated as the maximum point of the cross correlation, as shown in the lower plot. This has been determined to sub-channel accuracy by determining the center-of-mass of the peak above a threshold.

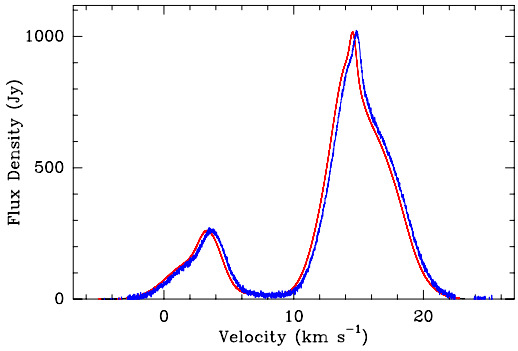

Figure 3-1: A synthetic 43 GHz maser with a flux of 6000 Jy km/s as observed by a ground station for 5 min. (red) and a satellite with a relative velocity of 317 m/s for 1 hr (blue). The velocity determination is accurate to 2.1 cm/s.

Fast Fourier Transforms (FFT) are commonly used to reduce the calculation time of the CC. According to the cross correlation theorem, CC in the spatial or time domain is equivalent to the multiplication of the complex conjugate in the frequency domain. Thus, instead of calculating the CC in the spatial domain directly, it can be calculated much faster by taking the FFT of the two signals, multiplying one by the complex conjugate of the other, and calculating an inverse FFT. That approach was taken in this work.

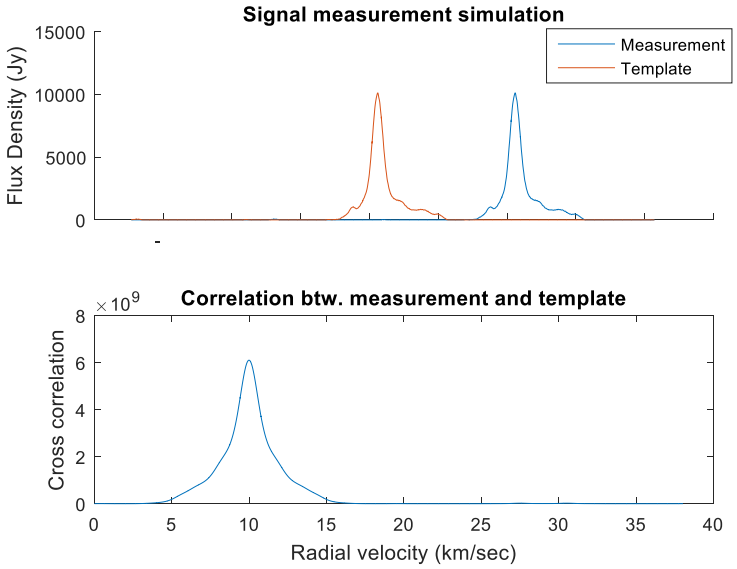

Fig. 3-2 Sample maser spectrum and cross correlation

Derivation: Cross-correlation as optimal peak position method

Let *g(n)* be the measured spectrum and *t(n)* be a template spectrum. Suppose that *g(n)* is some multiple *a* of *t(n)*, but shifted by an amount *s* and broadened by convolution with a symmetric function *b(n)* as following:

$$g(n) \cong \alpha t * b(n-s) \tag{3}$$

Where $*$ indicates convolution. The optimal shift is found by minimizing the cost function,

$$\chi^2 = \sum_n \left[\alpha t * b(n-s) - g(n)\right]^2 \tag{4}$$

Rewriting c^2 as

$$\begin{aligned} \chi^2 &= \alpha^2 \sum t * b(n-s)^2 - 2\alpha \sum t * b(n-s) g(n) + \sum g(n)^2 \\ &= \alpha^2 N \sigma_{t*b}^2 - 2\alpha N \sigma_g \sigma_t c * b(s) + N\sigma_g^2 \end{aligned} \tag{5}$$

where σ_g , σ_t , and σ_{g*t} are the root-mean-square (RMS) of the spectra,

$$\begin{aligned} \sigma_g^2 &= \frac{1}{N}\sum_n g(n)^2 \\ \sigma_t^2 &= \frac{1}{N}\sum_n t(n)^2 \\ \sigma_{t*b}^2 &= \frac{1}{N}\sum (t*b)^2 \end{aligned} \tag{6}$$

and *c* is the normalized cross-correlation function defined as

$$c(n) = g \times t(n) = \frac{1}{N\sigma_g\sigma_t}\sum_m g(m)t(m-n) \tag{7}$$

Minimization with respect to α yields

$$0 = \frac{\partial \chi^2}{\partial \alpha} = 2N[\alpha\sigma_{t*b}^2 - \sigma_g\sigma_t c * b(s)] \tag{8}$$

$$\alpha_{\min} = \frac{\sigma_g\sigma_t}{\sigma_{t*b}^2} c * b\left(s\right) \tag{9}$$

Substituting this value gives

$$\chi^2 = N\sigma_g^2\left(1 - \frac{\sigma_t^2}{\sigma_{t*b}^2}[c * b(s)]^2\right) \tag{10}$$

It follows that minimization of c^2 is equivalent to maximization of $\frac{1}{\sigma_{t*b}} c * b(s)$. If the broadening function is a Dirac δ function, c^2 is minimized by maximizing the cross correlation of

$$c(s) = g \times t(s) \tag{11}$$

3.2 Simulation results

3.2.1 Approach

The velocity estimation accuracy in the radial direction of the masers was estimated with a Monte-Carlo simulation of 10,000 observations processed with the cross-correlation approach. The assumed antenna and receiver specifications are described in Table 3-1.

Table 3-1 Antenna and receiver specification

Item	Parameter
Antenna area	1 m^2, 4 m^2
Receiver noise temperature	50 K, 100 K
Channel width	1kHz (13.6 m/sec in LSR velocity)
Antenna efficiency	0.5
Sampling efficiency factor	0.99
Signal integration time	600 sec, 3600 sec, 7200 sec

Table 3-2 lists the masers used in this simulation. New observations of H_2O maser spectra at MIT Haystack Observatory were compared to with archival spectra from the Mopra telescope in Australia acquired by the H_2O southern Galactic Plane Survey (HOPS), as well as SiO maser spectra measured at Mopra,.

Table 3-2 Maser sources for simulation

Source Name	Maser type (Telescope)	RA (J2000) (h:m:s)	DEC (J2000) (d:m:s)	Peak flux density (Jy)
G27.18-0.08	H2O (HOPS)	18:41:11.6	-05:08:53	3,932.7
G305.80-0.24	H2O (HOPS)	13:16:40.8	-62:58:24	3,023.5
G344.58-0.02	H2O (HOPS)	17:02:56.6	-41:42:13	1,266.3
ORION	H2O (Haystack)	05:35:14.5	-05:22:30	10,573.6
W75N	H2O (Haystack)	20:38:36.4	42:37:35	10,180.2
W3OH	H2O (Haystack)	02:27:04.7	61:52:24	
VY CMa	SiO (Mopra)	07:22:58.3	-25:46:03	484.78
Orion SiO	SiO (Mopra)	05:35:14.5	-05:22:30	360.4
W Hya	SiO (Mopra)	13:49:01.9	-28:22:03	349.69
L2 Pup	SiO (Mopra)	07:13:32.3	-44:38:23	219.68
Wx Psc	SiO (Mopra)	01:06:25.9	12:35:53	192.75
IK Tau	SiO (Mopra)	03:53:28.9	11:24:22	210.37
R Dor	SiO (Mopra)	04:36:45.6	-62:04:37.9	126.9

Figures 3-3 through 3-5 show the RMS error of the radial velocity estimation for each maser with the receiver specified in **Table 3-1**. The dotted lines bracket the minimum accuracy goal 0.5-1.0 m/sec. In general, it can be seen that the higher brightness H_2O masers are better suited to the target accuracy, which can be achieved after 2 hours with the 4 m^2 aperture but not the originally suggested 1 m^2 aperture. Implications of this finding are discussed in subsequent sections of this report.

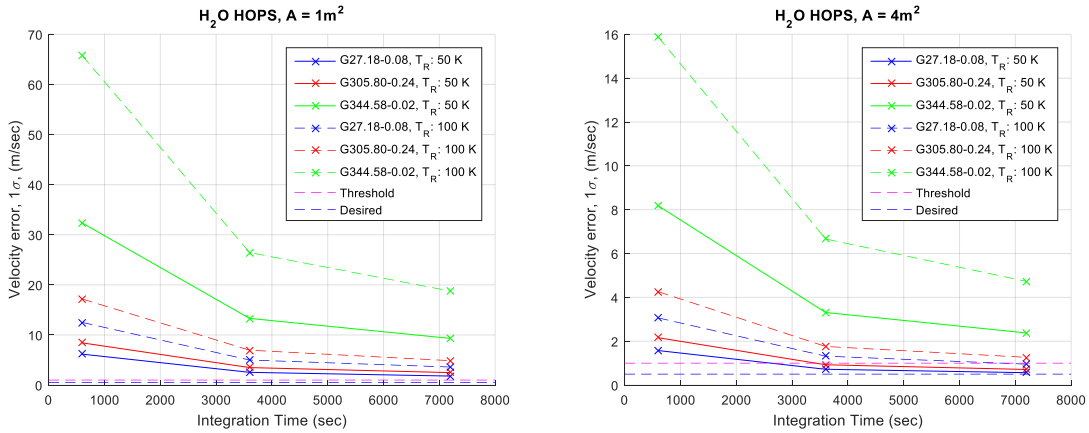

Fig. 3-3. Velocity estimation error simulated using H2O masers as observed at HOPS for telescope with A=1m^2 (left) and 4m^2 (right)

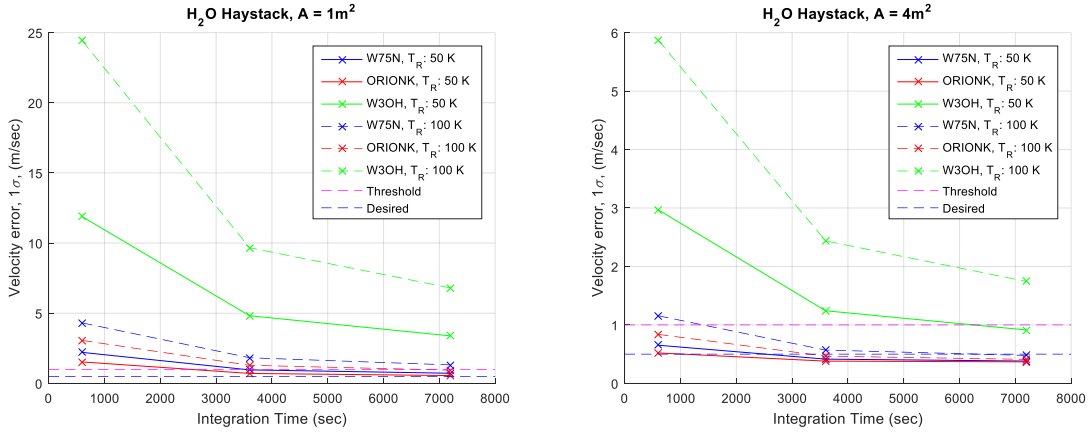

Fig. 3-4: Velocity estimation error simulated using H2O masers as observed at Haystack Observatory for antennas with A=4m^2 (left) and 1 m^2 (right)

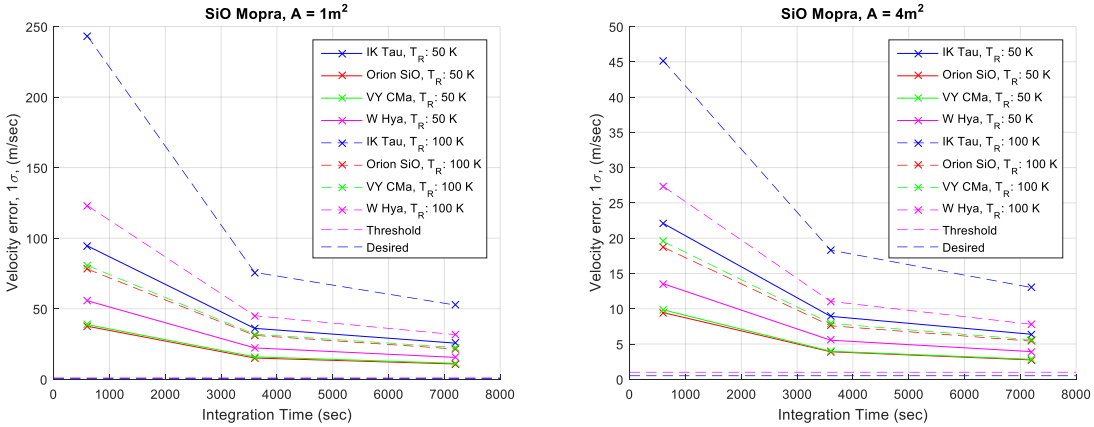

Fig. 3-5: Velocity estimation error simulated using SiO masers as observed at MOPRA for antennas with A=4m^2 (left) and 1 m^2 (right)

3.2.2 Limitations of the approach

As described in the introduction, only a single integration of a velocity vector is needed to estimate position, as compared to a double integration if an accelerometer is used. Here we discuss the degradation of position information resulting from that single integration, and confirm that the position error becomes arbitrarily large as the integration time increases.

Consider a spacecraft cruising without any internal or external source of acceleration, i.e. $\dot{r} = v = const$. Suppose that we know the exact initial position, r_0, and measure the velocity at a cadence of Δt with Gaussian white noise $n \sim N(0,\sigma_n^2)$, averaging N velocity measurements until the velocity estimate is arbitrarily accurate. Thus,

$$\hat{v}_N = \frac{1}{N}\sum_i v_i = \frac{1}{N}\sum_i (v + n_i) = v + m$$

where $m \sim N(0,\sigma_m^2)$ and $\sigma_m^2 = \sigma_n^2 / N$, and $\lim_{N\to\infty} \sigma_m^2 = 0$.

It follows that the position measurement will be $\hat{r} = r_0 + N\Delta t\hat{v}_N$ and the estimation error is:

$$e_r = r - \hat{r} = N\Delta t m \sim N(0,\sigma_e^2),$$

where $\sigma_e^2 = (N\Delta t)^2\sigma_m^2 = \sigma_n^2 N\Delta t^2$.

3.2.3 Simulation with covariance analysis:

Since the orbital dynamics are more complicated than a constant velocity model, we used Kalman filtering to analyze the variance of the position error over time. To simplify the problem, only gravitational force from the Sun is considered for the spacecraft's orbital dynamics,

$$\ddot{\vec{r}} = -\frac{\mu_s}{r^3}\vec{r}$$

where $\vec{r}$ is the position of the spacecraft in heliocentric frame and μ_s is the gravitational constant of Sun given as $\mu_s = 1.32712440018 \times 10^{11} km^3/\sec^2$. In the two-body orbital dynamics problem, the state to be estimated is

$$\vec{x} = \begin{bmatrix} \vec{r} \\ \vec{v} \end{bmatrix} = \begin{bmatrix} \vec{r} \\ \dot{\vec{r}} \end{bmatrix}$$

and its derivative is

$$\dot{\vec{x}} = \begin{bmatrix} \dot{\vec{r}} \\ \ddot{\vec{r}} \end{bmatrix} = \begin{bmatrix} \vec{v} \\ -\frac{\mu_s}{r^3}\vec{r} \end{bmatrix}$$

The partial derivatives (Vallado, 2007) are then

$$\frac{\partial \dot{\vec{x}}}{\partial \vec{x}} = F = \begin{bmatrix} 0 & 0 & 0 & 1 & 0 & 0 \\ 0 & 0 & 0 & 0 & 1 & 0 \\ 0 & 0 & 0 & 0 & 0 & 1 \\ -\frac{\mu_s}{r^3} + \frac{3\mu_s r_x^2}{r^5} & \frac{3\mu_s r_x r_y}{r^5} & \frac{3\mu_s r_x r_z}{r^5} & 0 & 0 & 0 \\ \frac{3\mu_s r_x r_y}{r^5} & -\frac{\mu_s}{r^3} + \frac{3\mu_s r_y^2}{r^5} & \frac{3\mu_s r_y r_z}{r^5} & 0 & 0 & 0 \\ \frac{3\mu_s r_x r_z}{r^5} & \frac{3\mu_s r_y r_z}{r^5} & -\frac{\mu_s}{r^3} + \frac{3\mu_s r_z^2}{r^5} & 0 & 0 & 0 \end{bmatrix}$$

The measurement is a partial velocity projected on the direction of the maser source as

$$v_m = \vec{m} \cdot \vec{v} + n_v = \begin{bmatrix} 0 & 0 & 0 & \vec{m}^T \end{bmatrix} \vec{x} + n_v = H\vec{x} + n_v$$

where $\vec{m}$ is the unit direction vector of a maser source, determined from the tabulated right ascension (RA) and declination (DEC), and n_v is the measurement noise for each maser source, assumed to be a Gaussian such that $n_v \sim N(0, \sigma_v^2)$. With the two sensitivity matrices, *F* and *H*, it is straightforward to apply the extended Kalman filter (EKF) to simulate navigation. Three H_2O bright masers (W75N, W3OH, and Orion) were used for the simulation, which was conducted for four different combinations of antenna size (1 and 4 m^2) and integration time (600 and 3600 sec), assuming a receiver temperature of 50 K. The noise variance of the measurement (s_v^2) for each maser was estimated from a Monte-Carlo simulation (Table 3-3).

Table 3-3 Maser sources used in the simulation and results for the four combinations of integration time and antenna aperture. s_v is given in units of m/s.

	W75N	**W3OH**	**ORION**
Peak flux density (Jy)	10,180.2	9,736.9	10,573.6
RA (J2000) h:m:s	20:38:36.4	02:27:04.7	05:35:14.5
DEC (J2000) d:m:s	42:37:35	61:52:24	-05:22:30
s_v 1 m^2, 600 sec)	2.208	11.882	1.527
s_v (1 m^2, 3600 sec)	0.961	4.820	0.708
s_v (4 m^2, 600 sec)	0.652	2.970	0.520
s_v (4 m^2, 3600 sec)	0.414	1.241	0.380

The impact of the cumulative error was estimated by simulating a Hohmann transfer orbit from Earth to Mars with a semi-major axis of ~1.25 AU (1.87×10^8 km). The initial OD error was set at 10 m in position and 1 m/sec in velocity, corresponding to 1σ of a Gaussian distribution. The simulation period was one million seconds, or approximately 11.6 days. The partial velocity measurement from the masers was updated with the same time step as its integration period, 600 sec or 3600 sec.

Since the variance of the measurement noise, which is due to thermal noise depending on the receiver temperature, is $\sigma_n^2 \propto \frac{1}{\Delta t}$, while the signal variance is $\sigma_e^2 \propto N\Delta t$, the SNR (and hence the position error variance) is expected to be effectively independent of the time step Δt for any given propagation time $T_p = N\Delta T$. In other words, one long measurement of velocity provides as much knowledge as many short measurements. This can be seen in Fig. 3-6, where 10-minute and 1-

hour measurements are compared. The slight variation between the two cases in the $4m^2$ simulation is due to the asymmetric shape of the maser spectra and the finite channel size of the spectral data.

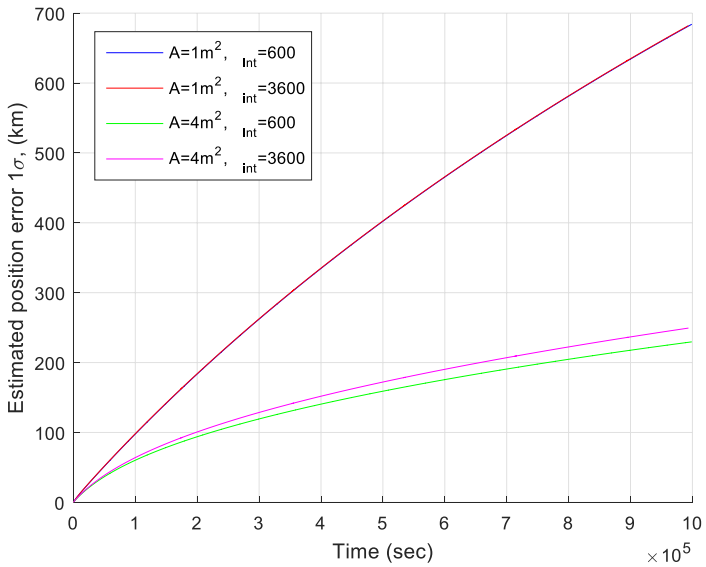

Figure 3-6 Estimated covariance of the position error for two integration times and antenna sizes, as a function of overall cruise duration. The cumulative error can be seen to be independent of integration time.

3.2.4 Simulation conclusions

The simulation results confirm that with a sufficiently large antenna, at least 4 m^2, and a low temperature (50K) receiver, it is possible to estimate a spacecraft's velocity with better than meter-per-second accuracy by observing bright water masers with peak flux > 10,000 Jy.

What remains to be determined is thus whether *actual* maser spectra are sufficiently stable and reproducible over time to achieve this theoretical accuracy. That is the subject of the following section.

4 Observations and analysis (masers)

Haystack's 37 m. radome-enclosed telescope is a world-class facility, well-suited for the observation of astronomical masers. The surface accuracy, drive mechanics, and support infrastructure have been completely refurbished in a 6-year campaign, and the telescope has been fully commissioned. The surface accuracy is better than 70 μm over a wide range of elevation, allowing the telescope to achieve near-maximal antenna efficiencies over its entire range of operating frequencies. At least 33% of the time is available for astronomy, concentrated in weekends and the daily midnight to 8am shift, with the remainder dedicated to radar observations under the auspices of MIT Lincoln Laboratory.

While the radar capabilities have been fully upgraded, the signal chain electronics are the same as were used before the renovation, and they are being gradually recommissioned. There are three dual-polarization receivers used for radio astronomy, in varying states of functionality: K band (22 GHz), Q band (43 GHz), and W band (86 GHz). Each receiver covers the frequency range of at least one transition of a bright, astrophysically important maser. Water masers at 22.235080 GHz are routinely observed with the K-band receiver. The Q- and W-band receivers cover several masing transitions of silicon monoxide, most notably at 43.122027 GHz and 86.243337 GHz.

A catastrophic power failure of the spectrometer early in the Tall Ship program resulted in an extended interruption of the measurements after the initial observations, and in the end we were only able to observe over a period of several weeks. This was sufficient, however, to assess short-term variability of spectral shape and to investigate Doppler ships at a low level of precisions.

4.1 Review of Literature

Prior to initiating new observations, the literature on bright masers was reviewed to support an initial decision on which maser type to observe, and to assess how much is actually known about short-term variability. On-line catalogs evaluated included Shintani, M. et al. (2008) and Valdettaro, R. et al. (2001), as well as published data such as those by and by Walsh et al. 2011, who surveyed 540 water masers at 22 GHz, and Breen et al. 2010, who catalogued 379 water masers, some of which are shown in Fig. 4-1.

An initial survey resulted in a decision to focus primarily on H_2O masers at 22 GHz, in K-band, rather than the initially proposed SiO masers at 43 GHz. It was concluded that new observations were necessary to quantitatively assess velocity shifts at the level of precision needed for this work, and candidate masers were selected from the surveys.

4.2 Target sources

Water masers are seen in a variety of astrophysical contexts including star-forming regions, the envelopes of evolved stars, planetary nebulae, and the centers of some galaxies. In star-forming regions, the 22 GHz water masers are often very bright and spectrally narrow, with individual maser spots having linewidths of a few hundred m/s or less. Individual maser spots often appear to be point-like at the typical resolution of a very long baseline interferometric (VLBI) array (about 1 milliarcsecond = 5 nanoradians). A star-forming region frequently contains more than one maser spot. Since these may be moving relative to each other, the observed spectra may have multiple Doppler-shifted peaks At the resolution of a single aperture, such as the Haystack 37m telescope or a spacecraft, all of the features are blended together into a single spectrum. The morphology of this spectrum can therefore range from a simple single peak to a complicated shape with many apparent peaks (Fig. 4-2).

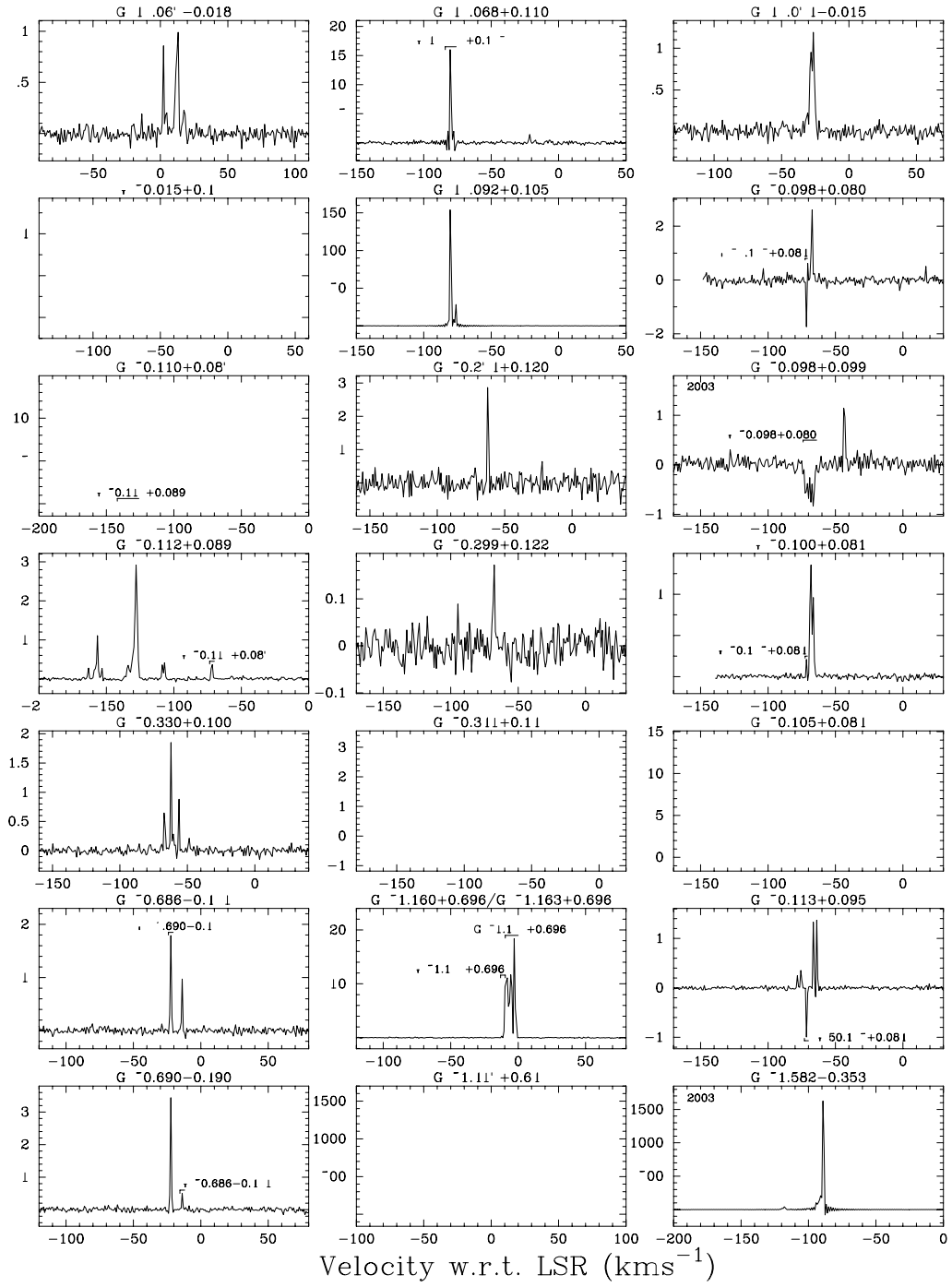

Fig. 4-1. Representative published spectra of water masers (Breen et al, 2010)

Maser spectra are observed to be variable over time periods of weeks and longer, although little data exists on shorter timescales. This variability can be due to a small change in the velocity centroid of a single maser spot or due to spectral blending of two maser spots whose intensities are changing relative to each other. For navigational purposes, the variability of maser features can be mitigated by ground-based monitoring to track and predict feature velocities.

The Haystack 37m antenna was used to observe several water maser sources over a time range of more than four months in 2015-2016 to examine the variability in feature velocities. The data were also used to characterize the potential performance of spacecraft systems as a function of the available aperture size. Since the Doppler shift $\Delta f = f*(v/c)$, a relative velocity increment of 1 m/s at 22.23 GHz results in a Doppler shift of 74.1 Hz. We therefore require stability from the telescope signal chain on the order of 10 Hz to obtain the desired accuracy.

Four water maser sources were ultimately selected for monitoring: Orion (RA 05:35:14.5 Dec -05:22:30.5, all coordinates J2000), W3(OH) (02:27:04.71 +61:52:24.6), Cepheus A (Cep A; 22:56:18.095 +62:01:49.45), and S269 (06:14:37.08 +13:49:36.7). These sources were all chosen because they have maser features that are at least several hundred Jansky in brightness (or significantly more in the case of Orion and W3(OH) and because they are up in the early morning hours during the winter at Haystack (latitude +42.6 degrees), when telescope time was available for this study. These four sources span a range of spectral complexity. The spectra of Orion and W3(OH) contain many very bright maser features that are spectrally blended, while Cep A and S269 each contain one isolated bright feature. The latter two are amenable to determination of the Doppler shift by cross correlation while the former would likely require some form of peak fitting, which may be a factor in design of flight avionics.

The Haystack spectrometer supports several observing bandwidths. Of greatest use for this project were the 5.9 MHz, 1.98 MHz, and 0.66 MHz modes, which span a velocity width of 80 km/s, 27 km/s, and 9 km/s, respectively. The observed bandwidth was channelized into 8192 spectral channels, providing a spectral resolution of 9.7 m/s, 3.3 m/s, and 1.0 m/s, respectively in the three modes. Even finer spectral resolution would be desirable for examining the stability of maser feature velocities, but the spectrometer currently deployed on the Haystack 37m telescope does not support narrower channels.

Radio telescopes often exhibit a bandpass response that is offset from zero or not flat with frequency. It is standard practice to observe with a bandwidth wide enough to include zero-signal channels at both ends, in order to fit and remove a baseline. The widest of these three observing bandwidths was necessary for Orion and W3(OH), for which the spanned velocity of the maser features is close to or greater than 27 km/s. All four sources were also observed in the two narrower-bandwidth modes, centered on the velocity of the brightest feature. The bandpass response was found to be flat in all cases.

For masers to be used as a frame of reference for velocities, it is important to demonstrate that their velocities are themselves stable. The apparent velocity of a maser feature at any given time from the surface of the Earth is Doppler shifted due to the rotation of the Earth and the Earth's orbital motion around the Sun. In order to test the potential velocity stability of maser features, sources were observed with Doppler correction, which introduces a compensating frequency shift in the local oscillator system.

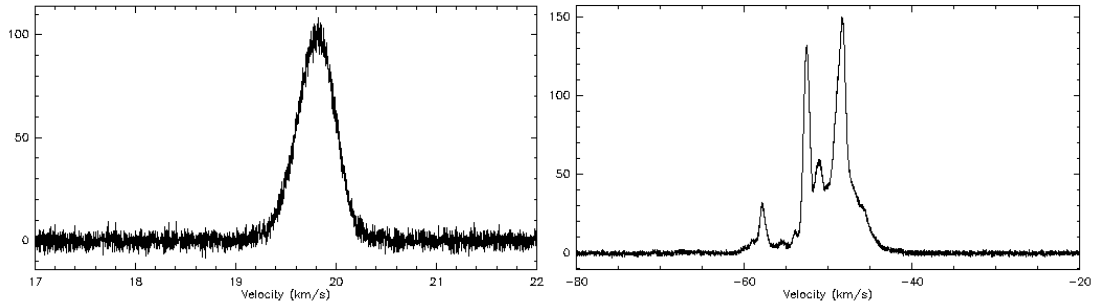

Fig 4-2. S269 (left) consists of one bright peak, while W3(OH) (right) is composed of many peaks.

4.3 Results

Maser signals are known to be unstable temporally, implying that the shape of the template may change over time. To the extent that relative amplitudes of the various peaks change, or some of the peaks of lesser interest shift due to internal motion of the stellar gases, then methods are called for that can distinguish component features in a complex manifold of peaks in order to extract the Doppler shift of a feature of interest. The most common approach is a nonlinear peak fit using, for example, the Levenberg–Marquardt algorithm**.** A wide array of software tools are available for nonlinear peak fitting; More sophisticated methods might include principal component analysis and target factor analysis. For complex spectra of this sort, the goal of this investigation is to identify the more stable features as well as the narrowest features, which typically (but not always) yield the most accurate determination of peak position.

To determine whether the maser spectra themselves are sufficiently stable to allow for spacecraft velocity determination, water masers were observed using the Haystack Observatory 37 meter telescope from October through January.As shown in Fig 4-3, the shapes of the spectra changed minimally over a period of 17 days, with changes most notably occurring in the relative amplitude of the component peaks rather than their relative frequency. This is as expected, and is easily accommodated by a fitting algorithm without compromising the accuracy of the Doppler determination. However, frequency shifts of the entire manifold approaching 20-30 m/s were also observed over the same period, an order of magnitude larger than the allowable tolerance. If real, shifts of that magnitude could be readily parameterized and uplinked to spacecraft on an occasional basis to provide fine corrections to the position solution. But a uniform shift of a manifold of peaks arising from separate emitting regions of a stellar atmosphere is not physically likely, and suggests that an instrumental artifact is responsible. To further explore this possibility, a set of spectra acquired on the same night were similarly analyzed (Fig. 4-4), since physical changes in the Doppler shift of the emitting region are less likely on short time scales. It can be seen that, indeed, similar variations on the order of 10-20 m/s were also observed in consecutive spectra. Continued work on improving the instrumental stability is thus needed to determine the underlying stability limit of the sources.

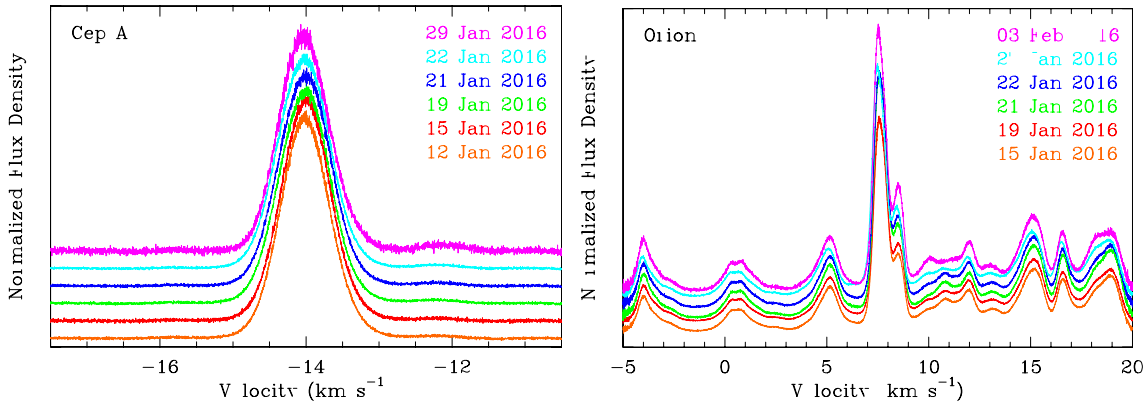

Fig 4-3. Left: Spectra of the Cep-A water maser at 22 GHz, acquired over a period of 27 days, showed no change of shape on a km/s time scale, but shifts in peak centroid position on a scale of tens of m/s. **Right:** Spectra of the complex water maser in Orion over the same period showed some change in relative amplitude of component structures, as expected, but frequency shifts affected all peaks (e.g. 27 Jan2016), suggesting instrumental artifacts.

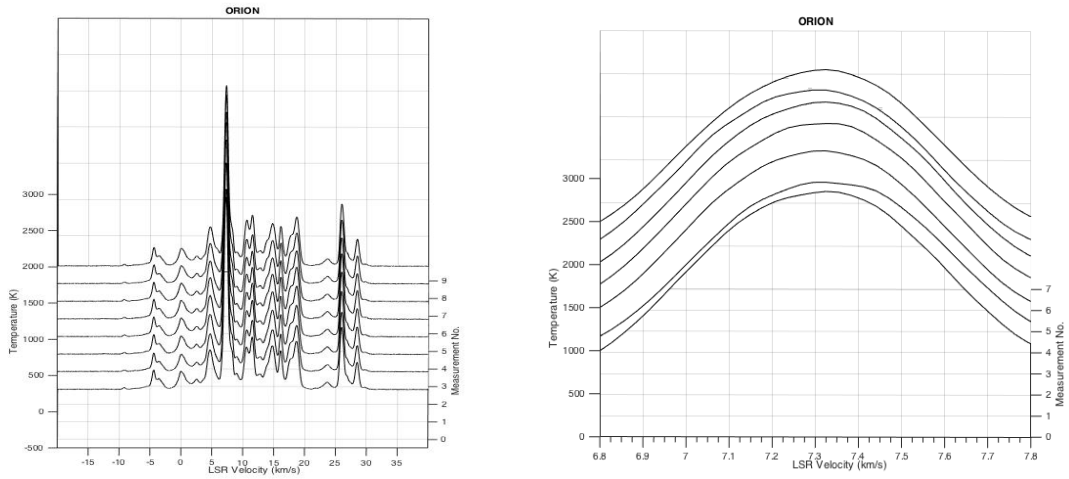

Fig 4-4: Spectra of the complex Orion water maser at 22 GHz, acquired over a period of several hours on Oct. 26, 2015, showed no significant change of shape (left), but close inspection reveals drift of peak position on a scale of 20-30 m/s (right). It is suspected that the variations are instrumental.

Peak fitting for this analysis assumed that the maser spectrum is a combination of Gaussian functions or, equivalently, Dirac delta functions broadened by a Gaussian distribution function. For the more complex Orion maser spectrum, we further constrained the component peaks such that their positions in frequency space are locked relative to each other such that, though the individual peak amplitudes may vary, the entire manifold is forced to shift left or right as a unit. This approach highlights the Doppler shift as the key variable, but is more general than a cross-correlation in that it allows for variation in the relative intensity of the emitting regions.

4.4 Conclusions from Observations

The overall conclusion is guardedly optimistic that the maser spectra themselves are sufficiently stable for navigation, with occasional ground support needed to update spectral parameters as originally postulated. While the variation in the peaks position is as large as $\pm$15 m/sec., which is much greater than the target of <1 m/sec accuracy, evidence suggests that the intrinsic variance is really much lower, with larger shifts due to an as-of-yet unidentified instrumental artifact. Those instrumental factors are currently being explored under separate funding.

5 Space-based RNAV validation (masers)

While the Tall Ship proposal described both the possibility of ISS validation, in analogy to SEXTANT/NICER, and a dedicated small-satellite demonstration, here we focus on a CubeSat-scale demo using a parabolic antenna, following the principle that if the technology can be accommodated in a CubeSat-class spacecraft, it is clearly practical for larger vehicles.

The nominal CubeSat implementation is intended to demonstrate minimum feasibility in a compact package. A conventional Earth-orbiting CubeSat would be assembled by the same group at MIT that developed the MicroMAS satellite (collaborator Cahoy). The data will be processed on board, referenced to a commercial chip-scale atomic clock (Lutwak 2012), and the resulting compact data set will be transmitted to Earth. Simultaneous observations from Earth will be compared to the CubeSat result, and the quality of the solution evaluated by comparison to independent navigation measurements.

5.1 Orbit considerations

In principle, the velocity of the spacecraft should remain constant over the integration time to avoid broadening the measured spectrum and compromising the accuracy of the demonstration. As an alternative, for a demonstration in Earth orbit, we would minimize the acceleration and compensate the remaining Doppler shift from a known model for each observation. In this case, the orbit determination (OD) of the spacecraft is of critical importance.

Several options were considered for space-based validation, including a high altitude circular orbit or lunar orbit, to approximate a free-space trajectory; and a highly elliptical orbit that would retain some aspects of a low acceleration trajectory apogee while still allowing use of commercial GNSS for precise orbit determination and high bandwidth download at perigee; or a readily-accessible low-Earth orbit.

A mission in low-earth orbit is also possible, and would benefit from the availability of GPS, but the orbital velocity swings through ~15 km/s over ~45 minutes, resulting in an average change in the Doppler shift of about 6 m/s per second. This could be addressed by de-chirping the raw data, mixing in the appropriate Doppler shift prior to the FFT. With a sufficiently accurate clock and an extra mix stage, this would allow coherent integration out to tens of minutes.

The choice was narrowed to two candidate orbits, one geostationary (GEO) and the second highly elliptical (HEO). GEO is advantageous in terms of accessibility since we can talk to the spacecraft continuously. If a satellite is in GEO, we can precisely determine its orbit on the ground by tracking with RF and uploading it for onboard Doppler correction during an integration. Also, the solid angle of Earth for a GEO satellite is 0.0179 sr (steradian), which is just 0.1426 % of the total celestial sphere, minimizing occultation problems compared to LEO. GEO orbits are, by comparison, in high demand and require considerable stationkeeping, though the upper and lower graveyard orbits provide a viable alternative.

A significant advantage of using HEO is the possibility of using an onboard GNSS receiver for near perigee, offering a significant cost advantage over ground tracking. In addition, ground communication from perigee imposes a substantially lower power penalty than at GEO, yet the satellite will spend most of its time observing near apogee, where Earth radio interference is reduced. Using a Molniya or Tundra orbit at an inclination angle of 63.4° (prograde) or 116.6° deg (retrograde) will minimize the burden of station-keeping for the propulsion system.

In summary, HEO offers a cost-efficient solution, requiring little or no propulsion, that can utilize GNSS for station-keeping and independent tracking. GEO offers the possibility of continuous observation and ground communication and a high accuracy OD solution.

For the purposes of this study, we will assume deployment of the spacecraft in HEO. The assumed orbital parameters are summarized in Table 5-1. Since the semi-major axis of the orbit is same as a geostationary orbit, the orbit period is 1 day, 24 hours.

Table 5-1: Baseline Orbit Parameters

Orbit Type	HEO
Semi-major axis (km)	42,157
Eccentricity	0.83464
Apogee (km)	70,972
Perigee (km)	600

5.2 Concept of Operations

Once the spacecraft is established on orbit, the mission supports five operation modes: Nominal Mode, Science Mission Mode, Orbit Determination (OD) Mode, Communication Mode, and Orbit Maintenance (OM) Mode. The phase of the orbit assigned to each of the operation modes is illustrated in Fig. 5-1. The following sub-sections describe each operating mode.

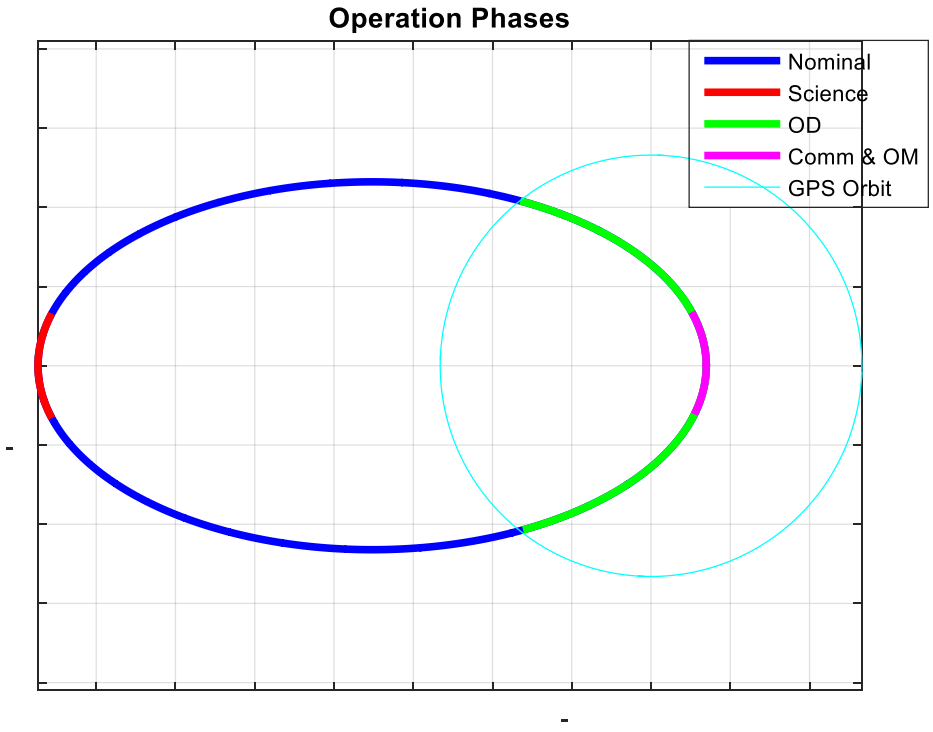

Figure 5-1 Operation phases in orbit, where (0,0) is Earth-centered. The blue, red, green, and magenta lines indicate Nominal, Science Mission, Orbit Determination, Communication, and Orbit Maintenance modes, respectively; the thin cyan line is the GPS orbit.

Nominal Mode: The spacecraft turns off payload, communications, and propulsion systems and points at the Sun with its solar panels to recharge the batteries. The total time length of this mode is 17.2 hours per one orbit, 8.2 hours each before and after Science Mission Mode. It takes 5.6 hours to fully charge the batteries.

Science Mission Mode: The spacecraft turns on the payload and points at the maser sources with the payload antenna. In this mode, the solar panel cannot point at the Sun, and will rely on the batteries for power. The orbit propagation will be used to determine the Doppler shift and the maser signal will be compensated prior to performing an FFT. The measured RF maser spectra will be used to determine the spacecraft's partial velocity in the direction of the maser source. The time period of Science Mission will be 4 hours per orbit, 2 hours before and after the apogee where the spacecraft's velocity is the most stable. We are considering 1 hour of signal integration time, so we will have up to three maser measurement opportunities, including the transition time to one maser source to another.

Orbit Determination Mode: The spacecraft is inside the GPS orbit, which is at an altitude of 20,200 km. In this mode, everything is the same as Nominal Mode except that the spacecraft is gathering position data from GPS signals and continuously performing precise orbit determination, either continuously with Kalman filtering or by Least-Square batch estimation at the end of the Orbit Determination Mode. The estimated epoch orbit in this mode will be used to determine the velocity of the spacecraft in Science Mission Mode. The Orbit Determination Mode period will be 2.8 hours per orbit.

Communication Mode: The spacecraft points the payload antenna to the ground station and downloads the science data through the X-band transmitter. The ground station checks the spacecraft status and uploads through UHF radio the measurement schedules for Science Mission Mode, and thruster firing schedules for Orbit Maintenance. Communication Mode is allocated a maximum of 26 minutes per orbit, when the spacecraft's altitude is lower than 2,000 km. The spacecraft will not gain any power from the solar panels at this time, as it is pointing to the ground, so it will rely on the batteries for power.

Orbit Maintenance Mode: The spacecraft fires its thruster to compensate the cumulated disturbances and maintain the target orbit. While Orbit Maintenance Mode can be initiated at any time that is optimal for firing, we expect this to occur primarily near perigee in order to compensate the aerodynamic drag and maintain the apogee altitude. The spacecraft attitude will be commanded to establish the ΔV direction, and no power will typically be generated from the solar panels.

5.3 Baseline Design

The spacecraft consists of two parts, the payload and bus systems. The payload comprises the maser signal detection and processing device, including the RF antenna, low-noise amplifier (LNA), and the hardware signal processing unit that performs the FFT.

The spacecraft bus system establishes the orbit and attitude for the maser measurement, points the payload antenna at maser sources, maintains a suitable orbit, and provides accurate velocity estimation to correct for the continuous, orbit-derived Doppler shift. It also provides power to the payload, and downloads science data to ground.

The design for the demonstration spacecraft bus system (TallCube) is based on KitCube, a moon orbiting 6U cube satellite for NASA's CubeQuest Challenge currently under development by MIT (Figs. 5-2 and 5-3). The total wet mass of KitCube is 11.7 kg, arranged in the traditional 3 x 2 x 1 U rectangular configuration. The system contains a Busek green monopropellant thruster system, and a thermal system, including four 10W heaters, 16 RTD temperature sensors, and eight copper thermal straps, which is used to mitigate the high operational temperatures produced by the propulsion system. In addition to a conventional RF communication system, KitCube features an optical communications payload, including a fine steering mirror for high laser pointing accuracy, which is to be used only for data transmission. KitCube will use the RF communication

to uplink and downlink data from NASA Wallops ground station, and will transmit optical communications data to the Optical Communications Telescope Laboratory ground station at NASA's Jet Propulsion Laboratory.

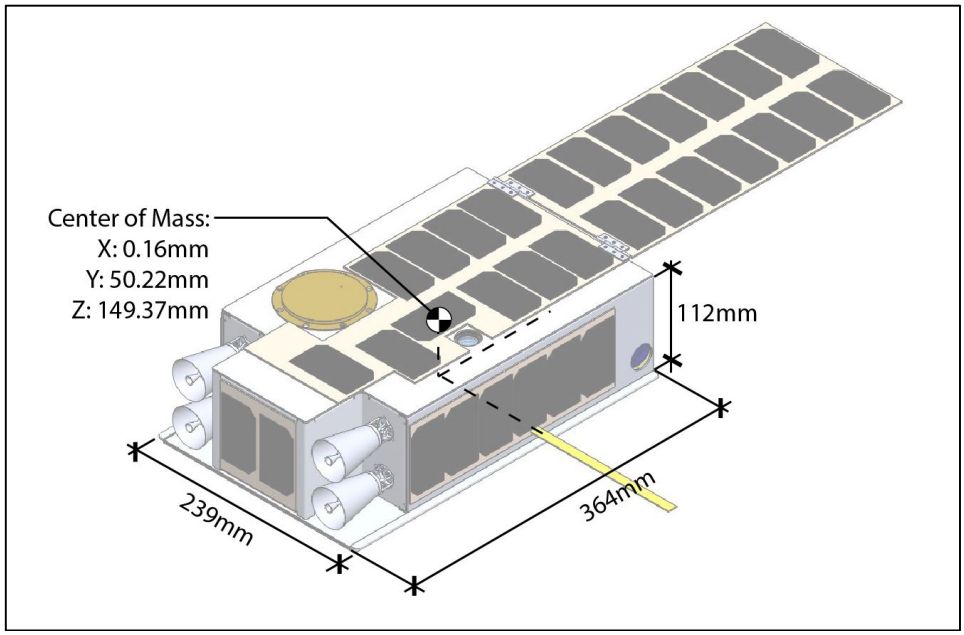

Figure 5 -2. Exterior view of KitCube

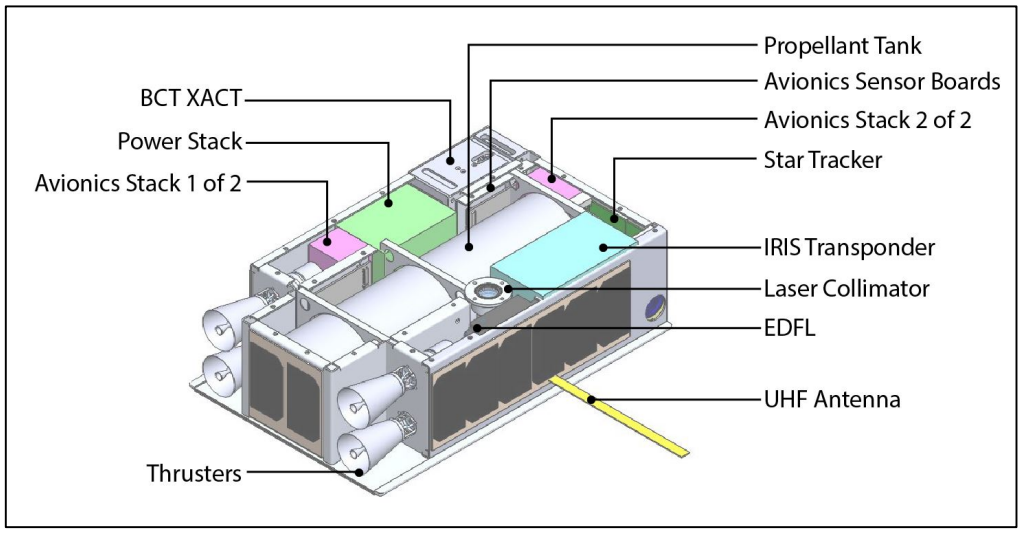

Figure 5-3. Interior view of KitCube

TallCube will be derived from the baseline KitCube design, without the optical communication capability. It will use X-band RF communications to download data, sharing the maser detection antenna (an architectural advantage of RNAV over XNAV). Other subsystems including the Attitude Determination and Control System (ADCS), power system, Avionics, structure, and propulsion will follow the KitCube design with only minimal modifications.

TallCube will use the same custom avionics bus as KitCube, and will also adopt the same suite of commercially available components for the ADCS, including a thin slice star tracker from Blue Canyon Technologies and six coarse sun sensors from SSBV Aerospace.

The baseline power subsystem consists of two 6U one-sided deployable solar panels and three 30 Whr Lithium-Polymer batteries, which are needed to sustain the spacecraft during the two-hour maser observation without recharging. 3G Flex EPS, a COTS EPS motherboard from Clyde Space, will be used to manage and distribute the system power.

The structure for TallCube has been designed in-house at MIT and will be made of sheet metal, which provides optimal system support and structural interfaces to system mechanisms, including those within the 6U solar panel deployer. The concept of operations for this mission will result in substantial radiation exposure; assessment and mitigation of this exposure has been marked for future work. The design will include radiation shielding for sensitive instrumentation, and current mass budgets allow for up to 1.35 kg of shielding material.

5.4 Subsystem Design

This section summarizes the design for key subsystems. Most of them are inherited from the KitCube design.

5.4.1 Communications

Table 5-2 shows key specifications for the communication subsystem, which, consists of a down-link-only X-band radio-frequency (RF) system and a bi-directional UHF RF system. The X-band transmitter is dedicated to downloading mission payload data, including the maser spectra measurement, while the UHF link will be used to exchange control command and housekeeping data. We are baselining the EWC 27 HDR-TM X-band transmitter from Syrlinks for X-band, and a Micron UHF radio that is currently being developed in-house, coupled with the UHF antenna. The X-band transmitter will share the 4 m^2 payload antenna, while the UHF will use its own monopole antenna.

Table 5-2. TallCube communication system specifications

	Syrlinks X-band Downlink	Micron Uplink	Micron Downlink
Purpose	Science data download	Command upload	Housekeeping data download
Comm. Band	8.025-8.4 GHz	391-464 MHz	391-464 MHz
Data Rate (Apogee)	50 Mbps	1.19 Mbps	57.2 kbps
Transmit Power	2 W	N/A	1 W
Weight	300 g	10 g	10 g
Total Power	10 W	0.5 W	5 W

5.4.2 Electrical Power System

The power subsystem will generate, regulate, store and distribute electrical power for all system loads during the mission. The baseline design includes two deployable one-sided 6U solar panels. Spring-loaded hinges deploy the panels to a 90° angle using a Clyde Space thermal knife driver. Maximum power is generated when the two panels point to the sun at the same time. Assuming 30% power conversion efficiency of the GaAs solar cells and an 0.8 packaging factor, each panel is expected provide 20 W when pointing directly at the Sun, for a total of 40W. A Clyde Space 3G Flex EPS and three 30-Whr Lithium-Polymer batteries will be used for power distribution and management, providing burst power up to 85 W during Science Mission and Data Download operation. Table 5-3 shows the power budget for each operational mode.

Table 5-3. TallCube power Budget

Subsystem	Nominal Op.	Science Mission	Data Download	Orbit maint.
Propulsion	0 W	0 W	0 W	60 W
ADCS	8.61 W	8.61 W	8.61 W	8.61 W
Avionics	0.2 W	0.2 W	0.2 W	0.2 W
Communications	0 W	0 W	15.5 W	15.5 W
Payload	0 W	20 W	0 W	0 W
Maximum DoD	N/A	36.44 %	75.38 %	75.38 %
Total	**8.81 W**	**28.61 W**	**24.31 W**	**84.31 W**

Since the TallCube mission orbit is highly elliptical with a period of 24 hours, the spacecraft will be in sunlight for at least 22 hours each orbit. Orbit maintenance and Data Download are performed near apogee, leaving 20 out of 24 hours for Nominal Operation, with the solar panel facing the Sun and the battery charging. Of the 40W generated power, 32W can be allocated to battery charging, and it only takes 5.6 hours to fully charge the batteries from 100 % depth of discharge (DoD). Table 5-3 also specifies the maximum DoD for each operation. Operation phase periods of 20 hours, 2 hours, 20 minutes, and 10 minutes are assumed for Nominal, Science Mission, Data Download, and Orbit Maintenance, respectively. Data Download and Orbit Maintenance are performed sequentially in eclipse, without an opportunity to charge the battery between the two operations.

5.4.3 Command and Data Handling

The Avionics Hardware subsystem consists of commercial off the shelf (COTS) components as well as custom developed interface boards. The driving requirements of the Avionics hardware is to provide power and data support to every component. The Micron Motherboard (MB), designed in-house at MIT for use with upcoming flight missions including MiRaTa and MicroMas-2, is based on the Pumpkin Motherboard, which has extensive flight heritage. Unneeded MHX and USB components have been removed from the Pumpkin MB, and the extra space used to install a backup UHF radio.

In addition to the MB, GlenAir, Inc. will provide three custom interface boards. These include a Communications Interface Board, an ADCS Interface Board, and a Propulsion Sensors Thermal Unified Devices (PSTUD) board. All three interface boards include Power Distribution Units (PDU's) to provide fault detection to the components. The Communications Interface Board provides power and data to the X-band RF transmitter and UHF Micron transceiver. Both the transmitter and the transceiver communicate with the bus through an SPI data protocol. The ADCS Interface board provides power and data to the XACT, star tracker, and sun sensors. The XACT uses 8V and 12V and will use the I^2C protocol to communicate with the Avionics Bus. The star tracker will run off 5V, and will connect directly to an XACT serial port to feed in inputs. The sun sensors also use 5V, and will send data to the Avionics bus over I^2C that will be forwarded to the XACT for attitude determination. The PSTUD interface board provides the interface to the Busek thruster, and will provide 5V and an RS-422 connection to the Busek PPU, which will control the thruster electronics and thrusters themselves. The PSTUD board also provides I^2C data connections and 3.3V to four heaters, a Pericom JT55 system clock, 16 temperature sensors, and two thermal knife drivers (TKD). A data block diagram is shown in Figure 5-4, and the ADCS is diagrammed in Figure 5-5.

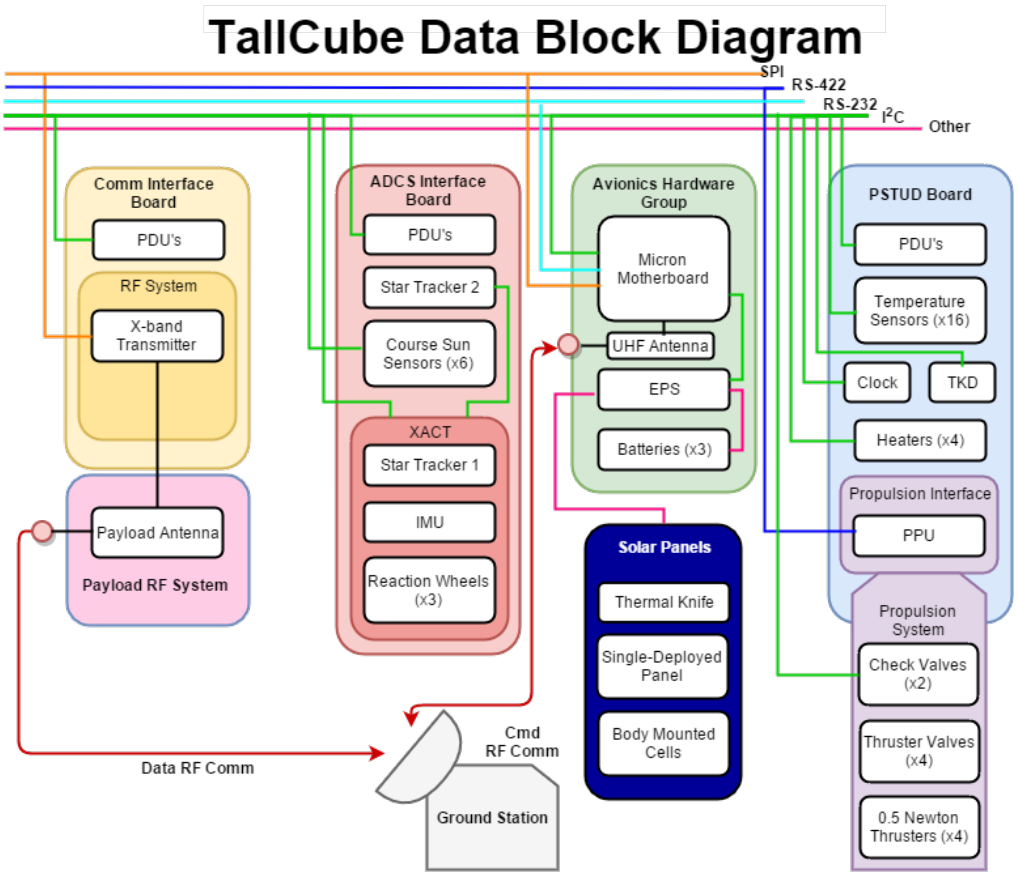

Fig. 5-4 TallCube Data Block Diagram

5.4.4 Guidance, Navigation, and Control

TallCube will use a parabolic deployable antenna for astronomical maser measurement. The driver for the Guidance, Navigation, and Control (GNC) subsystem is the requirement on payload antenna pointing control and accuracy. This, in turn, is derived from the Field-of-View (FoV) or the half-power beam-width of the antenna, which is determined from the following empirical equation (Wertz et al. 2011):

$$q = \frac{21}{f_{GHz} D}$$

where q is the beam width of an antenna in degree, f_{GHz} is the frequency in GHz, and D is the antenna diameter in meters. For a 2.25 meter diameter deployable antenna, the beam width is approximately 0.42°, requiring the spacecraft to provide attitude control accuracy better than 0.21°, or half the beam width. Attitude knowledge accuracy should be no worse than 10% of the control accuracy, which is 0.02° or 60 arcsec. This requirement drives the majority of the decisions made within the attitude determination and control system (ADCS).

TallCube must also maintain its attitude to within 1° while thrusting. Maintaining attitude control during thrusting is challenging because the net thrust is offset from the center of mass, so thrusting will apply a torque to TallCube. Additionally, differences in thruster performance will magnify this torque. To mitigate this problem, software will account for the expected torque and actuate the reaction wheels to counter it. Because the burns are short and the torque from the thrusters is large, the sensors will likely not react to the change in attitude quickly enough to totally nullify their effect.

To account for uncertainty and modeling errors, software components will include tunable parameters whenever possible. These will apply to extended Kalman filtering, sensor gains, spacecraft parameters, and thruster performance. This gives flexibility and will allow for the reduction of errors during the mission.

To precisely maintain attitude knowledge, TallCube is equipped with 6 course sun sensors (CSS), two orthogonal star trackers, and an inertial measurement unit (IMU). For attitude control, three reaction wheels from Blue Canyon Technologies (BCT) will be utilized. The thrusters will be used for reaction wheel desaturation, but they are not precise enough for attitude control. The IMU, one star tracker, and the reaction wheels are all present in the BCT XACT system.

The course sun sensors will be present on each face of TallCube to provide the most coverage. The sun sensors are from SSBV Aerospace & Technology, and they can provide course pointing knowledge to within 0.5°.

The two BCT star trackers have the same overall performance, but one is part of the integrated XACT system while the other is an external Thin-Slice Nano Star Tracker. A single star tracker can provide pointing knowledge to within 6 arcseconds about two axes, and within 40 arcseconds about the other (the star tracker's roll axis). The internal star catalog contains over 20,000 stars, and the star trackers can detect stars down to a 7.0 magnitude. Both also utilize internal baffles to restrict unwanted light. The baffle rejection is over 30dB within 2° of the camera field of view. Like all star trackers, however, there exist keepout zones for Earth, the Moon, and the Sun. This is 90° for the Sun and 54° for the Earth (Palo, et al., 2013). Due to this interference by celestial objects, two star trackers are necessary to confirm the availability of at least one during the science mission.

The BCT reaction wheels are housed in the XACT integrated system. Each wheel can provide 6 mNm of torque and store 15 mNm-s of angular momentum. This torque is sufficient to counter the torque caused by the net thrust and center of mass offset, which is required to maintain control during thrusting.

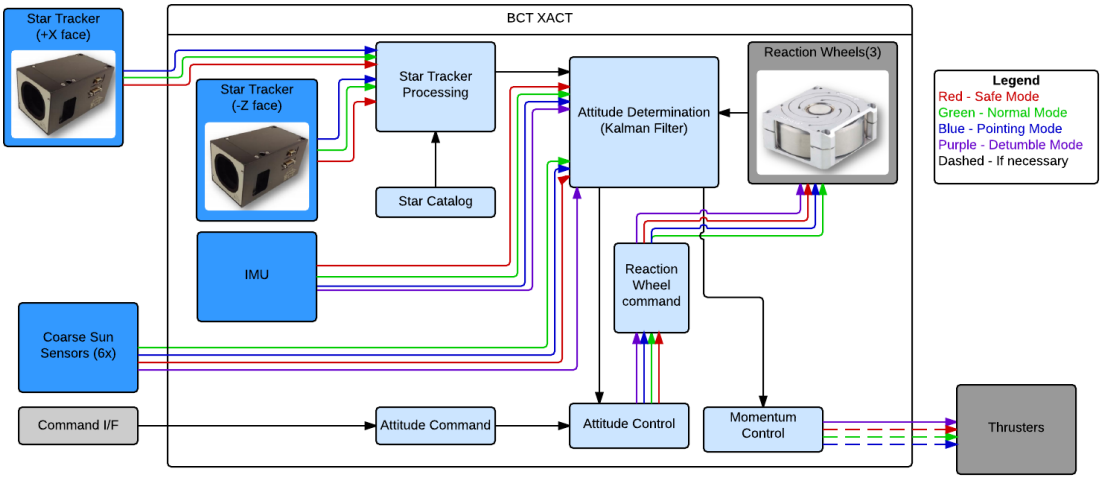

Figure 5-5. ADCS Hardware Block Diagram

Another requirement for the GNC subsystem is on orbit determination (OD). Because Doppler shift compensation is required to process the maser signal, GNC must provide accurate velocity estimates to the payload. Perigee of our HEO orbit is 600 km, which will allow us to utilize GPS or Galileo to determine the epoch. The GPSRM-1 GPS Receiver Module from Pumpkin will be used as the onboard GPS receiver (Fig. 5-6). It is expected to provide 10 m position accuracy and

1 m/sec velocity accuracy for each measurement. An extended Kalman filter will be implemented on-board to improve the orbit determination from the GPS data.

Figure 5-6. GPSRM 1 GPS Receiver Module

5.4.5 Structure

TallCube's structural subsystem will provide protection against launch loads and a suitable environment for the operation of all subsystems in all mission phases. The chassis assembly offers easy access to the data and power bus for debugging and assembly of components. The structural subsystem is required to carry, support, and mechanically align the spacecraft equipment, and it will also cage and protect deployable components during launch. The structural design of TallCube is largely inherited from KitCube. Figure 5-7 illustrates the exterior of TallCube structure design. Table 5-4 lists the mass budget of the TallCube bus.

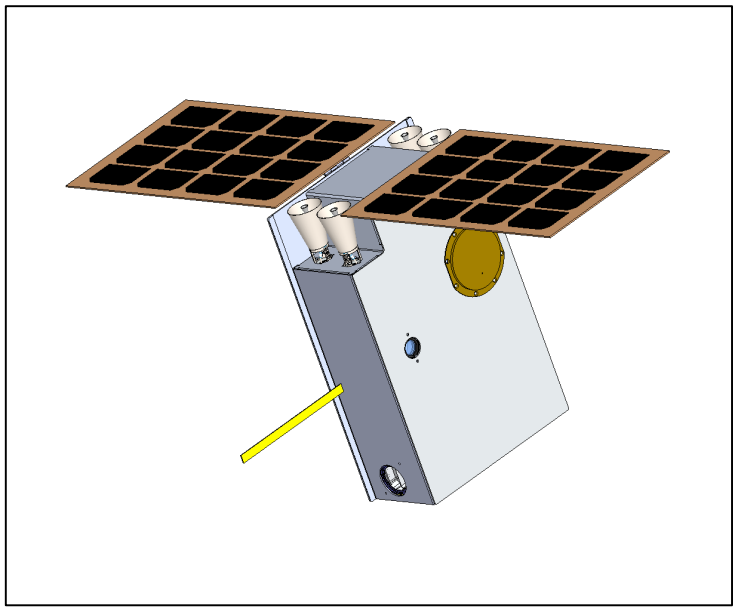

Figure 5-7. Exterior TallCube Bus System

Table 5-4 TallCube mass Budget (Spacecraft Bus Only)

Subsystem	Item	Mass (kg)
Propulsion	AF-M315E Propellant	2.05
Propulsion	Busek propulsion System	2.3
Propulsion	Moog 51E265 Latch Valves	0.5
Propulsion	Busek PPU and Sensors	0.15
Propulsion Total		**5**
Avionics Hardware	Micron MB	0.088
Avionics Hardware	ADCS Board	0.06
Avionics Hardware	Comm Board	0.06
Avionics Hardware	PSTUD Board	0.06
Avionics Total		**0.268**
GNC	XACT	0.85
GNC	Nano Star Tracker	0.35
GNC	Course Sun Sensor	0.03
GNC	GPSRM 1	0.1
ACDS Total		**1.33**
Structures	Chassis sheet metal	1.3
Structures Total		**1.3**
Communications	IRIS Radio	0.3
Communications	Micron Radio Board	0.01
Communications	UHF Monopole Antenna	0.01
Communications Total		**0.32**
Power	3G Flex EPS	0.148
Power	30 Whr Li-Polymer Battery	0.768
Power	Two 6U Deployable Solar Panel	1.0
Power Total		**1.916**
TallCube Totals		**9.866**

5.4.6 Propulsion

The proposed propulsion system for TallCube (Fig. 5-8) is a custom designed, green monopropellant system designed for KitCube and built by Busek Space Propulsion and Systems. The propulsion system is composed of four thrusters firing a highly stable green monopropellant, AF-5315E, developed by the Air Force Research Lab. This propellant provides a specific impulse of 220 seconds as well as increased stability and shock-resistance compared to other monopropellants. In addition to the four thrusters, the propulsion system also contains a propellant tank, two latch valves, four micropiezo valves, a PPU, propellant lines, and an array of sensors. The propulsion system has been designed to provide 390 m/s of delta-v in order to support the orbit correction and maintenance maneuver as well as desaturation of the reaction wheels. To meet NASA's triple inhibit requirement, each of the six valves in the system will be operated independently and have been placed in order to provide three seats between the tank and ambient for each thruster. In order to achieve sufficient performance, the tank will be pressurized to approximately 500 psi prior to launch.

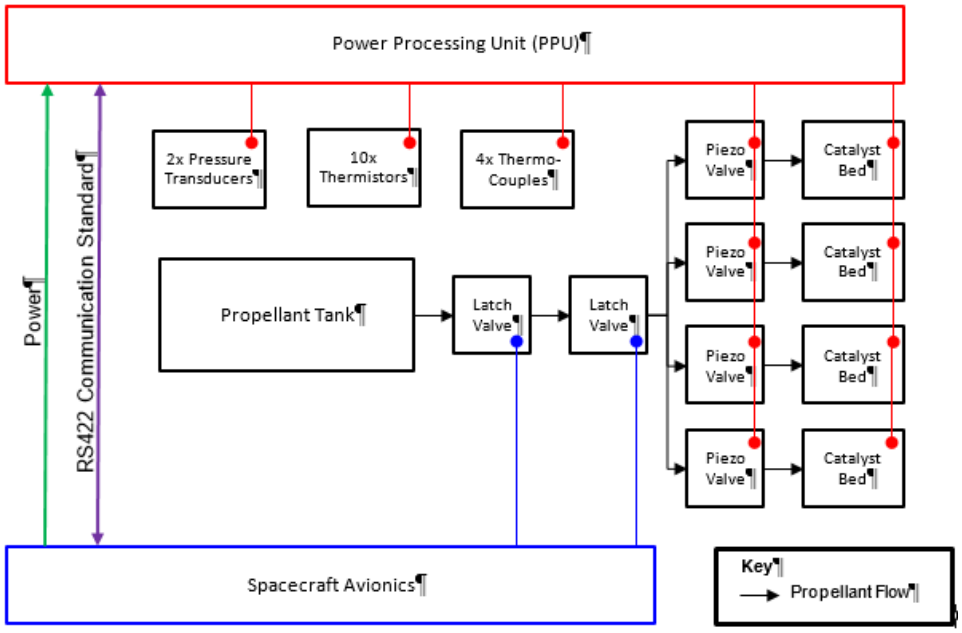

Figure 5-8. Propulsion Subsystem Block Diagram

5.5 Antennas

Depending on spacecraft architecture, navigational requirements, synergistic uses of antennas and antenna structures, and the path of technology, future RNAV users will be able to choose among phased arrays (Hansen 2009), next generation reflectarrays (Huang and Encinar 2008), and large deployable reflectors.

5.5.1 Trades

Phased arrays: Phased array systems for high frequencies have recently been developed using SiGe RF beamforming architectures. In these architectures the antenna pattern is synthesized before the receiver using integrated RF phase shifters and combiners. This is currently the most commonly used architecture in defense and commercial systems. Specific challenges faced for a space based 40-80 GHz array primarily have to do with relatively wide RF bandwidth requirements and scaling challenges. It will be necessary to selecting an approach that scales to a large enough collecting area and addresses packaging issues for platforms with limited surface area (e.g. cubesat). A low cost approach would be to adapt phase array receiver chips developed for automotive radar (24, 77, 79 GHz) or WiFi applications (60 GHz). A multiple receive beam architecture would be implemented to increase observation speed through duplication of the analog beamforming network. Digitization of the output signals would be accomplished using conventional A/D converters with limited bit depth, or using single bit digitization architectures if necessary to minimize power consumption and complexity. A high performance clock is necessary for stabilization of the A/D converter (and other array oscillators) to achieve the required spectral stability (~ 1 part in 10^{12} to 10^{13} depending on frequency). A chip scale atomic clock may be used for centimeter per second level measurement while a more advanced deep space atomic clock would be needed for higher levels of performance. Conventional FFT or Sparse FFT approaches would be used for processing the RF signal. The spectral analysis would be done using conventional computing, FPGA, or ASIC approaches.

An optimal maser application for phased arrays might observe the SiO line at 43 GHz (λ=7 mm), allowing for an implementation with commercial technology. Currently available systems in that band have 16 antenna channels per chip. Typical filled array spacing is 0.65λ, so approximately 40,000 elements are needed to populate a square meter filled aperture. Cost per channel is currently $10-$25 per channel, or at least $400K for the square meter array for the ISS demonstration. Costs are as low as $1 per channel in silicon, consistent with a typical CubeSat budget, but the noise figures are still relatively poor.

Power consumption is a more immediate resource challenge for phased arrays, possibly as high as 250 mW per LNA channel but plausibly as low as 50 mW in a custom design. This suggests an array power of at least 2kW during operation. From an energy perspective, this is acceptable with a 1:100 duty cycle, plausible for a navigation instrument, but appropriate storage batteries would have to be be included in the power system design.

Reflectarrays: Reflectarrays have been integrated into small solar panels, either on the back side of the panel or in a transparent configuration on the front (Huang and Encinar 2008). Technology developments in three areas will determine whether reflectarrays supplant phased arrays as the optimal solution for a flat antenna. The first is beamforming, which depends on tuning the individual elements with MEMS switches or phase shifters. This allows for electronic tuning without the power penalty of an array of individual LNAs. The second is active surface control, which will enable larger arrays than is currently possible while maintaining submillimeter flatness. The third development is in the fabrication area, where experiments in 3D printing of the surface promise a future flexible, low-mass implementation that can be integrated with the spacecraft structure.

Parabolic antennas: New developments in deployment of large structure from CubeSat-scale spacecraft promise to allow the continued use of conventional antennas even in a small format vehicle. This technology offers the most promise for pulsar detection in the short term, since at long UHF wavelengths the spatial tolerances are substantially relaxed and the antenna can be a coarse mesh. It is more challenging but still feasible for short wavelength applications.

We anticipate three generations of such designs in the future:

1. Passive structures that maintain surface quality through rib boom stiffness. This requirement determines the thickness of the rib material, how tightly it can be stowed, and thus the size of the deployment mechanism. Such an antenna can readily be built today, but maintaining surface tolerances for large diameters is challenging.
2. Antennas with active surface quality control, implemented by embedding actuators within the ribs and spokes. The component technology is expected would be available fairly soon that will enable the actual engineering design and qualification. We anticipate that the such antennas will be flight-ready within ~5 years.
3. Antenna booms that are built in space using 3-D printing. With this approach, the ideal rib boom shape can be created with minimal surface errors. The booms can be very thin because they don't have to tolerate a gravity field, and the shape can be made precise without the need for embedded control mechanisms.

5.5.2 TallCube design choice

In light of the near-term challenge of fabricating 4 m^2 reflectarrays to the required tolerances, and the power challenges of phased arrays of comparable size, the TallCube design choice is a deployable parabolic antenna using technology developed by our partner Stellar Explorations, Inc.

The TallCube design is based on what has become a fairly standard method of deploying flexible, rolled up ribs. A flexible reflecting surface (a metallized polymer such as Kapton) is stretched between those ribs, which are stowed for the launch on a spool and and unwound during deployment (Fig 5-9).

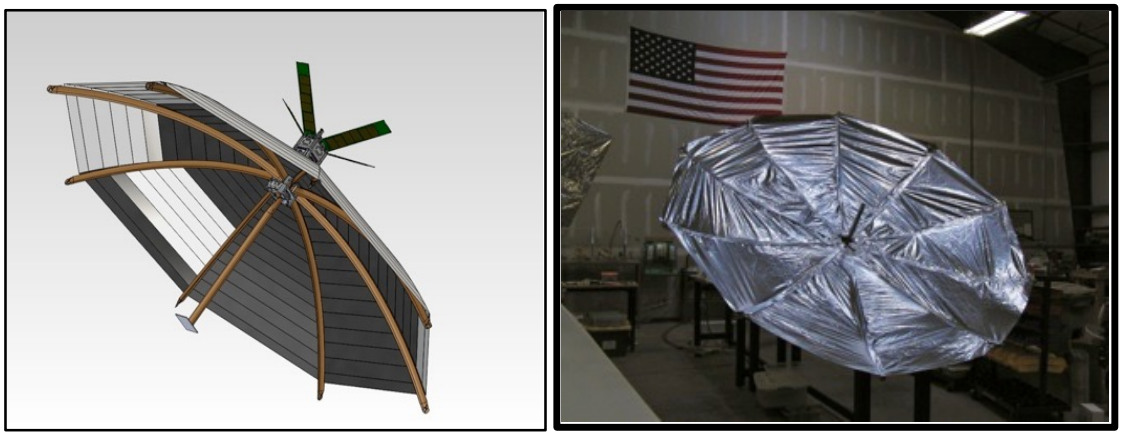

Figure 5-9. Stellar Exploration, Inc. deployable parabolic antennas.

5.6 Signal processing

The challenge in designing avionics for radio science is to find a compromise between the relatively power-hungry electronics typically use in ground-based telescopes (notably the products of the CASPER project) and the limited resources of small spacecraft. More specifically, the goal might be to port the mature CASPER designs to newer low-power FPGAs and A/D converters, at least to the extent that these are available in appropriately radiation hard formats, in order to achieve high spectral resolution at low power. Such avionics might be further streamlined by introducing newer, more efficient algorithms such as those for sparse FFTs.

The key electronic component of the radio receiver is the low noise amplifier (LNA), which itself utilizes only ~125 mW but requires removal of ~200mW heat that could demand ~7W electric using a miniature cryo-cooler. Down-conversion requires an additional ~1W and digitization uses ~2W for a converter and ~2W for the FPGA, for an overall total of ~12W prior to any signal processing. Signal processing power has been estimated by loading a CASPER project spectrometer design into Xilinx power estimation tools and switching to the FPGA we expect will be used for a Tall Ship application.

For non-electronic scanning, spacecraft pointing will be required to keep the beam on the maser. Doppler shifts associated with known motions (e.g. spacecraft orbit) may be removed from the RF signal in the FPGA prior to spectral estimation and integration.

For H_2O masers the center frequency is 22.235 GHz and assuming our target masers are W75N, W3OH, and ORION, the range we need is roughly -100km/sec to +100km/sec, corresponding to $\pm$7.4117 Mhz. For this application we assumed a channel width of 1kHz, corresponding to a Doppler shift of ~10 m/s.

6 The case for pulsars

A Tall Ship and a Star to Steer Her By ("Tall Ship") was motivated by the NICER/SEXTANT (N/S) flight project that, as part of an X-Ray Astrophysics experiment on ISS, expects to demonstrate some of the principles of autonomous X-Ray Navigation (XNAV) using pulsar timing. NICER/SEXTANT uses a large, precision x-ray telescope intended primarily for Astrophysics as a proof of concept of a small, specialized navigation system. N/S is deployed on the International Space Station (ISS), so while it has little fidelity to such a dedicated system, it nonetheless has the advantage of independent positioning information and capable power, timing, telemetry, and computing resources. Results from N/S can then be scaled downward to arrive at the minimal capable XNAV system.

For RNAV, pulsar signals are strongest at lower frequencies, but both antenna size and certain noise sources also increase at lower frequencies, and temporal broadening due to scattering goes up as the observing frequency goes down. As a result, there is a "sweet spot" for observation that is typically in the range 300-1000 MHz. Archives of pulsar measurements in this frequency range are listed in Table 6-1.

Table 6-1. On-line archives of UHF pulsar spectra.

Telescope	Frequency	Reference
Ooty	327 MHz	http://adsabs.harvard.edu/abs/2015ApJ...804...23K
Arecibo	327 MHz	http://adsabs.harvard.edu/abs/2013ApJ...775...51D
LOFAR	<200 MHz	http://adsabs.harvard.edu/abs/2015A%26A...576A..62N
Green Bank	350 MHz	http://adsabs.harvard.edu/abs/2013IAUS..291...41L

6.1 Approach

At the time of submission of the Phase I proposal, the literature suggested that a capable UHF pulsar-detection system required of order 100 m^2 antenna aperture, and imposed mass and power requirements that stretched the capability of small satellites (Becker et al. 2013). More recent studies out of the same group (Jessner et al. 2016) now suggest that the power and computational issues are modest, and smaller antenna sizes of 30-40 m^2 will be sufficient for detection. Moreover, at the recommended frequency of ~500 MHz, the antenna may consist of a lightweight mesh, and surface errors of 5-10 cm can be tolerated.

As a result, we can consider relatively flimsy structures for UHF pulsar detection that weigh no more than K-band antennas for maser detection and are substantially more tolerant to distortion. From a system perspective, this may prove simpler and less resource-intensive to implement, with superior navigational results. As was discussed for masers, the antenna might be a phased array, reflectarray, or a deployed parabola, but the parabolic shape is more favorable in the short term.

While pulsar spectra follow a power law that strongly favors long-wavelength detection, at sufficiently long wavelength the cosmic radio background dominates. As a result, the optimal operating frequency for pulsar-based RNAV is in the UHF. The need for large antennas in this range can be somewhat offset by using the greatest possible bandwidth for signal acquisition (a practice that is also adopted for VLBI geodetic observations, see Petrachenko 2009). In space, far from terrestrial sources of interference, that bandwidth can be as large as 50% of the center frequency.

The best sources for position determination have a large radio flux, narrow pulses, and a high duty cycle (i.e. short period) to maximize the integrated signal. Millisecond pulsars that meet this

requirement are sufficiently distributed across the sky to allow for spacecraft position and velocity to be determined in three dimensions. Since the measurement is based on time-of-arrival (TOA), the position vector to any single pulsar is redundant with the period of the pulsar, equivalent to ~1000 km. Simple inertial tracking between measurements can eliminate this redundancy.

The most recent and relevant assessments of navigational capabilities with pulsars are those of Jessner et al. (2016) and of Brito et al. (2015). Both analyze performance with a specific set of known pulsar characteristics, and both are substantially more optimistic than prior estimates.

To *first order*, timing accuracy from a set of such measurements varies as:

$$\sigma_{x1} \propto \frac{1}{A_{ant1}\sqrt{BT_{int1}}} \tag{6-1}$$

where A_{ant} is the antenna area, B is the bandwidth, and T_{int} is the integration time.

In practice, some inefficiencies are introduced as any of these parameters increases: A larger antenna area is more prone to physical distortion and requires more precise pointing; larger bandwidth introduces dispersion correction overhead and error; and increased integration time introduces smearing as the spacecraft moves and accelerates. But the general relationship allows us to extrapolate the particular modeled values and to perform system-level trades of performance as a function of allocated resources such as system mass and volume, pointing accuracy, and observing time (which translates into energy usage). At a minimum, this crude method allows us to select design parameters for more rigorous modeling.

Thus, for example, Brito et al (2015) conclude that an antenna with A=10 m^2 can establish position accuracy of 10.5 km in only 2.8 minutes by observing five pulsars with a bandwidth of 400 MHz at 1 GHz (B1937+21, B0329+54, B1933+16, B2020+28, and B1642-03). In addition to examining pulse width and SNR, Jessner et al (2016) consider jitter and broadening of the pulse by the interstellar medium, and they include the challenge of correcting for dispersion with near-continuous FFTs in their system resource analysis. They conclude, however, that a 50 m^2 antenna might be sufficient to determine spacecraft position to an accuracy of 1 km (equivalent to 3.3 μs timing accuracy) with a bandwidth of 50% at a center frequency of 500-550 MHz by observing four pulsars for 1 hr (J1909-3744, B1937+21, J0437-4715, and J1713+0747). This estimate results in an antenna sized at 2.5x the area of the Brito et al. (2015) value, and the authors caution that it might be low by nearly a factor of two.

Both methodologies imply that parabolic antennas with diameters ranging from 1-10 m can be expected to determine spacecraft position with accuracy from 1-10 km. To compare these results, Table 6-2 applies equation (6-1) to scale the test cases to a common set of cases of interest. Further economies could be realized by observing multiple sources simultaneously with a phased array, which may offset some of the power and computational penalty. The observing time would essentially scale inversely with the number of beams.

Table 6-2: Estimated antenna size needed to achieve 1 and 10 km positioning accuracy for integration times of 1, 5, and 20 hrs, extrapolating values in Brito et al.

(2015) and Jessner et al. (2016). The top two rows are the scenarios evaluated in the two references; subsequent rows are extrapolated using Equation (6-1).

			Brito et al (2015)		Jessner et al. (2016)	
Accuracy (km)	Int. time (hrs)	Bandwidth (%)	Area (m^2)	Diameter (m)	Area (m^2)	Diameter (m)
10.5	4.67	40%	1	1.1		
1	1	50%			50.0	8.0
1	1	25%	28.7	6.0	70.7	9.5
1	1	50%	20.3	5.1	50.0	8.0
1	5	25%	12.8	4.0	31.6	6.3
1	5	50%	9.1	3.4	22.4	5.3
1	20	25%	6.4	2.9	15.8	4.5
1	20	50%	4.5	2.4	11.2	3.8
10	1	25%	2.9	1.9	7.1	3.0
10	1	50%	2.0	1.6	5.0	2.5
10	5	25%	1.3	1.3	3.2	2.0
10	5	50%	0.9	1.1	2.2	1.7
10	20	25%	0.6	0.9	1.6	1.4
10	20	50%	0.5	0.8	1.1	1.2

6.2 In-space validation

By analogy to the N|/S demonstration of XNAV, it might be argued that for RNAV, an ideal demonstration would utilize a capable, if large, radio telescope, preferably in a high orbit (i.e. with a slowly changing velocity vector), with low noise electronics and independent, high precision position information. Fortunately, such a system not only already exists, but it is producing both pulsar and maser data of the sort needed to evaluate the RNAV concept.

Radio Astron is a 10-meter space-based telescope in a high orbit designed largely for Very Long Baseline Interferometry (VLBI) (Kardashev et al 2012. Designed primarily for Very Long Baseline Interferometry (VLBI), Radio Astron is equipped with high precision timing and its absolute position is known to great accuracy. Laser ranging determines its range to <10 cm and, by virtue of its VLBI activities, its absolute position within its 65-70 km orbit is known to high precision.

At 327 MHz, RadioAstron can observe two 16-MHz channels, while at 1.6 GHz, it can observe four 16-MHz channels. These channels are Nyquist sampled at 1 bit; because the phase of the signal is effectively random, correlation with a second ground-based antenna is necessary to detect pulsars from the 1-bit measurement. Moreover, the total data rate is small because the data have to be transmitted back to the ground for correlation against ground stations. For a pulsar navigation mission, the measurement would be at least 12 bits deep, bandwidth would be as large as possible,and processing would be performed on-board.

With an aperture of ~80 m^2, Radio Astron is only a factor of 2-3 larger in area than the size expected to be needed for pulsar detection. Receivers at 92 and 16 cm wavelengths bracket the bands likely to be useful for pulsar-based RNAV, and higher frequency receivers can be used for maser studies. Bit-depth and bandwidth are limiting factors, as Radio Astron was designed for VLBI activities, but total flux monitoring should provide adequate information for our purposes.

As part of the Phase 1 effort, we spoke with Dr. Michael Johnson at the Smithsonian Astrophysical Observatory, a co-investigator on Radio Astron, and identified a number of productive strategies for utilizing existing Radio Astron data to explore RNAV feasibility. These include studies

of highly stable millisecond pulsars as well as brighter, longer period pulsars that provide poorer timing fidelity but can be detected with even smaller antennas.

Use of Radio Astron data as a single-dish flux detector takes advantage of a subtlety of the pulsar and maser signal characteristics. RadioAstron is designed for VLBI applications, where the signal (visibilities) appear only as a result of correlation of the noise signal with a ground-based antenna. To minimize telemetry load, the RadioAstron data digitization is only 1-bit deep and, since the arrival phase is essentially random, without correlation across a baseline it shouldn't be possible to observe an amplitude pulse at all! Fortunately, a total flux measure can be extracted by using knowledge of the dispersion properties of the pulsar chirpto essentially autocorrelate the data as a function of frequency. The maser spectrum is similarly recovered via FFT. Examples of pulsar and maser detection are shown in Figures 6-1 and 6-2, respectively. As from Earth, the maser signals are considerably brighter than pulsars, but contain less navigational information.

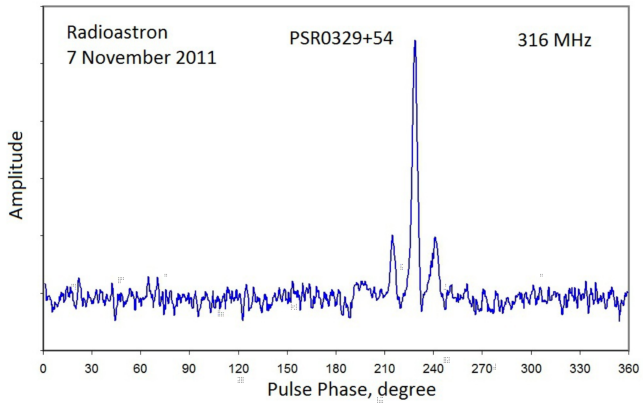

Fig. 6-1. RadioAstron observations of the bright pulsar PSR0329+54 at 316 MHz, after averaging 90 minutes of data. The amplitude is in arbitrary units. "Pulse phase" refers to TOA with respect to a nominal reference within the pulsar period. (*Data courtesy RadioAstron Pulsar Working Group*).

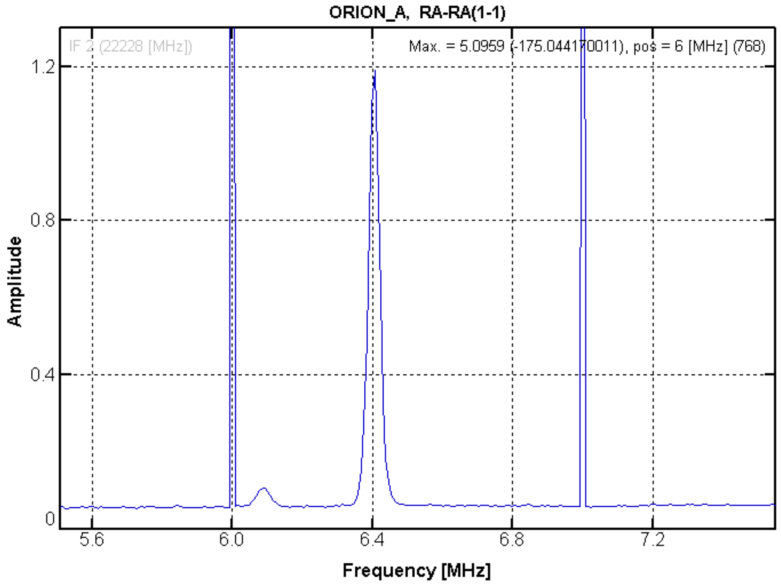

Fig. 6-2. RadioAstron space telescope observation of the water maser in the Orion KL region with right circular polarization at 22 GHz. The high narrow peaks on either side correspond to the pulse-calibration signal. Amplitude is in arbitrary units. (*Data courtesy RadioAstron pulsar working group*).

Should a Phase II effort be awarded, we intend to independently demonstrate determination of Radio Astron position using only existing or new pulsar timing data, as a flight implementation that fully leverages existing assets. To extend the result to a small system (RadioAstron weighs 5000 kg), we will extrapolate the performance to a multi-bit amplitude measurement and determining the optimal bit depth. We will assess the quality of this navigation data and use the result to define the requirements of a compact system compatible with small spacecraft. If possible, the RadioAstron demonstration will be done in coordination with XNAV measurements from NICER/SEXTANT, which welcomes such collaboration (*Keith Gendreau, private communication*).

There is no single solution to autonomous navigation. Rather, as with most spacecraft challenges, an arsenal of tools including XNAV, RNAV with masers and pulsars, optical navigation, inertial measurements, and ground support will be brought to bear, optimized for any given mission objective and requirements. With Tall Ship, we intend to advance that art, ultimately to let the marketplace of ideas and exploration determine the best course.

7 References

Anderson, K.D., Pines, D.J., *Experimental Validation of Pulse Phase Tracking for X-ray Pulsar Based Spacecraft Navigation*, Proc. AIAA Guidance, Navigation, and Control (GNC) Conference, 5202 (2013)

Arzoumanian, Z. et al. 2014, Proc. SPIE 9144, *Space Telescopes and Instrumentation 2014: Ultraviolet to Gamma Ray*, 914420 (2014)

Becker, W., Bernhardt, M.G., & Jessner, A., *Autonomous Spacecraft Navigation with Pulsars*, proceedings of Relativistic Positioning Systems and their Scientific Applications, arXiv:1305.4842 (2013)

Breen, S.L. et al, *Water masers accompanying OH and methanol masers in star formation regions,* Mon. Not. R. Astron. Soc. 406, 1487–1532 (2010).

Brito, D., Tavares, G. and Fernandes, J., *Radio Pulsar Receiver Systems for Space Navigation,* In 8th European Symposium on Aerothermodynamics for Space Vehicles, 2015, European Space Agency (ESA), Lisbon, Portugal, March 2015 (2015)

Curkendall, D. W. & Border, J. S., *Delta-DOR: The One-Nanoradian Navigation Measurement System of the Deep Space Network --- History, Architecture, and Componentry*, The Interplanetary Network Progress Report 42-193, 1-46 (2013)

Dong, J., *The Principle and Application of Maser Navigation*, arXiv:0901.0068 (2011)

Hansen R. C., *Phased Array Antennas*, Wiley (2009)

Huang, J. and Encinar, J., "Reflectarray Antennas," Institute of Electrical and Electronic Engineers, J. Wiley & Sons (2008)

Jessner, A., *Technical requirements for autonomous spacecraft navigation using radio pulsars*, To appear in the proceedings of the 593rd WE-Heraeus Seminar on Autonomous Spacecraft Navigation, Bad Honnef , Germany, June 8 - 11, 2015

Kardashev, N.S., Kovalev, Y.Y. Kellermann, K.I., *RadioAstron: An Earth-Space Radio Interferometer with a 350,000 km Baseline*, Radio Science Bulletin, 343, 22-29 (2012)

Lutwak, R., *At the Frontiers of Time*, GPS World. 23, #12, 44-45 (2012).

M. Micci and A. Ketsdever, ed., *Micropropulsion for Small Spacecraft*, AIAA Progress in Aeronautics and Astronautics Series, 187,52 (2000)

Petrachenko, B. (chair), *Design Aspects of the VLBI 2010 System*, NASA/TM-2009-214180 (2009)

Plag, H.-P. and Pearlman, M. ed., *Global Geodetic Observing System*, Springer-Verlag (2009)

Powell, D. , *Lasers boost space communications*, Nature 499, 266–267 (2013)

Shintani, M. et al., *Statistical Properties of Stellar H2O Masers --- Results of Three-Year Single-Dish Observations with the VERA Iriki Telescope*, Publications of the Astronomical Society of Japan, Vol.60, No.5, pp.1077—1131 (2008)

Valdettaro, R et al., *The Arcetri Catalog of H2O maser sources: update 2000*, Astron. Astrophys., 368, 845-865 (2001)

Vallado, D., *Fundamentals of Astrodynamics and Applications*, Springer (2007)

Walsh, A.J. et al, *The H2O Southern Galactic Plane Survey (HOPS) – I. Techniques and H2O maser dat*a, Mon. Not. R. Astron. Soc. 416, 1764–1821 (2011).

Wertz, J.R., Everett, D.F, Puschell, J.J. Eds., *Space Mission Engineering: The New SMAD*, Microcosm Press, 2011